Available online at www.sciencedirect.com
SCIENCE DIRECT®
Journal of Computational Physics 205 (2005) 408–438
JOURNAL OF COMPUTATIONAL PHYSICS
www.elsevier.com/locate/jcp

Quasi-neutral fluid models for current-carrying plasmas

Pierre Crispel [a,b,c,*], Pierre Degond [a], Marie-Hélène Vignal [a]

[a] MIP, UMR 5640 (CNRS-UPS-INSA), Université Paul Sabatier, 118, route de Narbonne, 31062 Toulouse Cedex, France
[b] CNES Centre de Toulouse 18, avenue Edouard Belin, 31401 Toulouse Cedex 4, France
[c] ONERA Centre de Toulouse 2, avenue Edouard Belin, 31055 Toulouse Cedex 4, France

Received 22 April 2004; received in revised form 18 November 2004; accepted 18 November 2004
Available online 19 December 2004

Abstract

In this paper, we propose three formulations of a model describing a quasi-neutral plasma with non-vanishing current. These formulations are obtained by exploring the quasi-neutral limit of a two-fluid isentropic Euler system coupled with the Poisson equation. In order to study and compare the numerical efficiency of each formulation, two test-problems are implemented in one dimension. The first one is a periodic perturbation of a uniform stationary plasma. The second one is a case of plasma expansion in vacuum between two electrodes.

1. Introduction

1.1. Modeling of quasi-neutral current-carrying plasmas

In this paper, which is a continuation of an earlier work [8], we are interested in the modeling of an unmagnetized quasi-neutral two-species plasma constituted of electrons and one ion species. A first possible description of this plasma is by means of the two-fluid Euler–Poisson system, which consists of the Euler equations for each species coupled by the Poisson equation. For this model, an important dimensionless parameter is the ratio of the Debye length to the typical size of the device. The Debye length measures the typical scale over which charge unbalances can occur and, for this reason, must be resolved by the numerical mesh size. Therefore, when this parameter is small, which is very often the case, numerical simulations require huge computational resources. In practice, multi-dimensional simulations and even, in

* Corresponding author. Tel.: +33 5615 26952.
E-mail addresses: crispel@mip.ups-tlse.fr (P. Crispel), degond@mip.ups-tlse.fr (P. Degond), mhvignal@mip.ups-tlse.fr (M.-H. Vignal).

0021-9991/$ - see front matter © 2004 Elsevier Inc. All rights reserved.
doi:10.1016/j.jcp.2004.11.011

some cases, one-dimensional simulations of this model are difficult to achieve. To overcome this problem, quasi-neutral models are routinely considered. Such models are formally obtained from the two-fluid Euler–Poisson system by letting the ratio of the Debye length to the typical size of the device tends to zero.

Quasi-neutral plasmas may carry a non-zero current. For unmagnetized plasmas, the assumption of zero-current is often made. In this case, the quasi-neutral model is very similar to the usual gas-dynamics Euler equations. If however the current is not supposed to be zero, the form of the quasi-neutral model differs significantly. The goal of this paper is to explore some numerical resolution methods in this case. Physically, this situation has been widely studied and we refer to [44] and references therein for a review. Mathematically, the quasi-neutral limit has been rigorously investigated for current-free plasmas ([7,49] for instance), but to our knowledge, the current-carrying case is still open. Therefore, we shall limit ourselves to formal arguments.

In the current-carrying quasi-neutral limit, the two-fluid Euler–Poisson model reduces to a two-fluid Euler model where the electric field is implicitly determined by the quasi-neutrality constraint. This formulation can be re-written by formulating the quasi-neutral constraint as a divergence-free constraint for the current. In this way, the electric potential can be explicitly determined by an elliptic equation. This corresponds to a first formulation of the quasi-neutral model which we call "constrained two-fluid formulation". Then, this system can be reduced successively to what shall be referred to as the "1.5-fluid formulation" and the "one-fluid formulation" by combining the different conservation equations. These systems are constituted of a hyperbolic part and a source term. The successive reductions from the constrained two-fluid formulation to the 1.5 and one-fluid formulations are performed by moving some terms from the source term to the hyperbolic part of the system by means of the quasi-neutrality constraint. Therefore, these manipulations change the hyperbolicity condition of the operator associated to the hyperbolic part. Indeed, this operator is strictly hyperbolic in the constrained two-fluid formulation, not strictly hyperbolic in the 1.5-fluid formulation, and conditionally hyperbolic in the one-fluid formulation. Moreover, the one-fluid formulation which has been largely studied in [15] is ill-posed in multi-dimensional cases. We shall stress the formal equivalence of these formulations: they are equivalent ways to write the same quasi-neutral model but each formulation leads to different numerical schemes with different efficiencies. These schemes are called constrained two-fluid, 1.5-fluid and one-fluid schemes.

The study of the different scheme efficiencies is the main point of this work. This is the reason why we work in this paper on two test-cases which are mono-dimensional.

The first test-case consists of a periodic perturbation of a quasi-neutral uniform stationary plasma with a non-zero current. For this test-case, we can compute the exact solution of the linearized problem about a steady state. For small perturbations, the solution of the non-linear problem is believed to be close to the solution of the linearized problem. Then, for each formulation, we compare the corresponding analytical solution of the linearized problem to the numerical solution of the non-linear problem. Furthermore, this study gives conditions of linear stability. Indeed, unstable cases correspond to the two-stream instability (see e.g. [5]) which occurs in high current plasmas.

The second test-case is a case of plasma expansion between two electrodes in vacuum. A large density plasma is emitted at the cathode and undergoes a thermal expansion. At the plasma–vacuum interface, electron emission occurs in the Child–Langmuir regime (see e.g. [5,11,12,18]) and generates a current inside the plasma. The device is then divided in two adjacent zones: a quasi-neutral plasma zone with non-zero current and an electron beam. This phenomenon and particularly the coupling of these two different zones has been thoroughly studied in a series of works [13–16] in relation with high-current plasma diodes [54] and arcing on satellite solar cells [6,19,39]. The goal here is to compare the numerical efficiency of each formulation in a physical situation.

For both test-cases and for each system, the numerical method in one dimension is based on a time splitting: the hyperbolic part of each system is first resolved by a Godunov scheme [23]. Then, the source terms are taken into account by an implicit Euler scheme coupled with the divergence-free constraint for the

current. For the plasma expansion case, since the quasi-neutral plasma has an interface with the electron beam, an interface tracking method is implemented with an adaptive mesh.

The paper is organized as follows. We first develop the physical context in Section 1.2. Then, in Section 2, we introduce the two-fluid Euler–Poisson model in the multi-dimensional case and the formal derivation of the quasi-neutral model formulated by the constrained two-, 1.5- and one-fluid systems. In Section 3, numerical schemes associated to each formulation are detailed. In Section 4, the test-case of perturbation is described and the accuracies of the different schemes are compared. In Section 5, the plasma expansion test-problem is described and the numerical schemes are compared. The proofs of technical results are collected in Appendix A.

1.2. Physical context

In this section, we discuss in greater detail the applications we have in mind. The first application deals with high-current plasma diodes [30,34,45,54,57]. High current plasma diodes are used for various applications such as high power micro-wave generation, free electron lasers, and material surface treatment. These devices have been designed to produce intense electron beams. Conventional electron guns cannot emit currents beyond the Child–Langmuir limit [31] because the space-charge layer in the vicinity of the cathode reflects the emitted electrons. However, if a plasma is formed at the cathode and expands towards the anode, this limitation can be bypassed. Indeed, the electron emission now develops from the plasma–vacuum interface, which is closer to the anode than the actual cathode. In the mean time, the plasma being a highly conductive medium, the potential drop in the plasma is negligible and the overall potential drop is now supported by the gap between the anode and the plasma–vacuum interface. The Child–Langmuir current, which is proportional to $V^{3/2}/L^2$, where V is the cathode to anode potential and L is the cathode to anode distance, increases as L now stands for the plasma– vacuum interface to anode distance. This distance decreases with time as the plasma expands in the gap and the extracted current is continuously increased, until the plasma shortcuts the electrodes.

In practice, the plasma is formed by the explosion of the cathode material (see e.g. [45]). The explosive emission mechanism has been reviewed in [33], as well as in [30,34]. The cathode protrusions locally generate large electric fields and electron field emission occurs at the tips. The Joule heat released at the tip contributes to its melting and vaporization and a neutral cloud is formed. The neutrals are then ionized and an ionization sheath is formed. Additional cathode heating is provided by the bombardment of the ions formed and accelerated in the sheath. The characteristics of the plasma are difficult to measure and vary significantly with the distance to the cathode [33] but it seems that the electron temperature does not exceed a few electronvolts. The modeling of the cathode plasma expansion can be made by using the methods proposed in the present paper, in particular those developed for the plasma expansion case (second test-case). The physical problem studied here bear strong analogies with the ion sheath problem, which have received much interest [1,22,24,42,43,46–48,53] and references therein. The question of boundary conditions at sheath edges has been numerically investigated in [37]. We also note that the kinetic analysis of a plasma bunch has been performed in [29].

A second example where the present methods can apply is the modeling of arc formation on satellite solar generators. Power on satellites is generally provided by solar generators which use semiconductor solar cells to convert solar radiation energy into electrical power. Solar generators consist of individual solar cells of about a few cm^2 in surface, which are connected in series into 'strings' to provide the required potential difference (usually ranging from 50 to several hundreds of volts). Strings are then connected in parallel to deliver the requested power to the satellite equipments. Solar cells are made of high quality semiconductor materials (usually Germanium) and are very expensive to fabricate.

It happens too often that after a certain operation time, an entire portion of the solar generator undergoes a permanent failure. The reason for it is the occurrence of an electrical arc which shortcuts one or several strings.

The scenarios for arc formation on satellite solar generators have been widely investigated [6,25–28,38,50,51,56]. According to this scenario, the satellite charging in the earth environment plasma triggers a primary discharge between a cell interconnect and the dielectric which is used in the protective layer. The so-created plasma plume expands and eventually connects and shortcuts two neighboring solar cells. The potential difference between the two cells (which is generated and maintained by the operation of the cells themselves) induces the transition of the primary discharge into a secondary arc. Once this arc is established, it pyrolyzes the insulating kapton substrate and transforms it into a conductor, which provides a permanent solid-state shortcut between the two cells, thereby irremediably deteriorating this part of the solar generator. The initiation and development of the primary discharge have been modeled in [6,19,39]. The second phase of the discharge scenario, namely the expansion of the plasma plume and the transition from the primary discharge into the secondary arc can be modeled by using the methods presented here and particular those dealing with the second test-case (plasma expansion case).

We now discuss the validity of the fluid description of the plasma. Indeed, this description is only correct if collisions are frequent enough to relax the distribution function to a Maxwellian equilibrium; otherwise, a kinetic description is necessary, as in [29]. A good measure of the collision efficiency is the temperature relaxation rate which, for Coulomb collisions, depends on the plasma density and temperature [3,52]. For both the plasma diode case and the solar cell case, the temperature is estimated to a few electronvolts (the neutrals ionization potential). The plasma density (which is difficult to measure) can be estimated to 10^{19} m^{-3} in the diode case [33] and to 10^{21} m^{-3} in the solar cell case [50]. A typical time scale of the device operation is the ion transit time in the gap, the latter being about 10^{-1} m wide in the diode case and 10^{-3} m in the solar cell case. With these figures, the product of the temperature relaxation rate by the typical time scale of the device operation is the same in both examples: a few tens for ions, and a few thousands for electrons. For electrons, this number is large enough for the fluid description to be meaningful. It is more questionable for ions, but one can think that turbulence and microscopic inhomogeneities in the plasma will increase this figure by some unknown factor, which makes the fluid description acceptable, if not fully justified. One should mention that the fluid calculations are by orders of magnitude faster than kinetic ones, and can at least be considered as valuable first guesses which need to be ultimately confirmed by fully kinetic simulations.

A definite way to assess the validity of the fluid description would be by comparing it with a collisional kinetic theory approach. However, stochastic codes using the Monte-Carlo method [35] develop a large amount of numerical noise which makes it difficult to accurately capture fast transient phenomena. Deterministic codes [2,4,10,20,21,36,40,41] certainly provide an interesting perspective but would necessitate specific developments which are outside the scope of the present work.

Several other points require some discussion, such as the absence of neutrals or the neglect of electron–ion collisions. Indeed, if the temperature is a few electronvolts, the plasma is likely to be only partially ionized. Similarly, if electron–electron and ion–ion collisions are frequent enough to bring the particle distributions to equilibrium, electron–ion collisions should be included as well. Both could easily be accounted for. In the same vein, one could discuss the isentropic assumption, which constrains the temperature to be a power law of the density. Obviously, this assumption is not entirely correct, since fast, hot electrons can reach the front of the plasma from the cathode. We have actually extended our work to Euler models including energy equations [9], allowing for a better account of energy and heat transport. However, the goal of the present paper is to provide an algorithmic and numerical perspective, rather than a fully exhaustive physical point of view.

2. Three formulations of a quasi-neutral model for current-carrying plasmas

In this section, we study the quasi-neutral limit in the two-fluid Euler–Poisson system. To this aim, the Euler–Poisson system is scaled and the formal limit leading to the quasi-neutrality is explored. This limit leads to a single quasi-neutral model that has several formally equivalent formulations.

2.1. The two-fluid Euler–Poisson model

We denote by $m_{i,e}$ the masses of ions and electrons, $n_{i,e}$ their densities, $u_{i,e}$ their velocities and $q_{i,e} = \pm q$ their charges where $q > 0$ is the elementary charge. The particle pressure laws are assumed isentropic and are given by $p_{i,e} = c_{i,e} n_{i,e}^{\gamma_{i,e}}$, where $\gamma_{i,e} > 1$ are the ratio of specific heats and $c_{i,e}$ are given constants. The temperatures are given by $T_{i,e} = p_{i,e}/n_{i,e}$. Moreover, ϕ is the electric potential.

On a domain $\Omega \subset \mathbb{R}_d$, $d = 1, 2,$ or 3, the particle conservation laws are given by $\forall x \in \Omega,\ \forall t \in \mathbb{R}_+^*$,

$$(n_i)_t + \nabla \cdot (n_i u_i) = 0, \tag{2.1}$$

$$m_i\left[(n_i u_i)_t + \nabla \cdot (n_i u_i \otimes u_i)\right] + \nabla p_i(n_i) = q n_i E, \tag{2.2}$$

$$(n_e)_t + \nabla \cdot (n_e u_e) = 0, \tag{2.3}$$

$$m_e\left[(n_e u_e)_t + \nabla \cdot (n_e u_e \otimes u_e)\right] + \nabla p_e(n_e) = -q n_e E, \tag{2.4}$$

and the electric field $E = -\nabla\phi$ is given by the Poisson equation

$$-\varepsilon_0 \Delta\phi = q(n_i - n_e), \tag{2.5}$$

where ε_0 is the vacuum permittivity. If we denote by n_0 the scale of the plasma density and by T_0 the scale of the plasma temperature (in units of energy), we recall that the Debye length λ_D, which is the length scale where electrostatic interactions occur in the plasma, is given by

$$\lambda_D^2 = \frac{\varepsilon_0 T_0}{q^2 n_0}. \tag{2.6}$$

The numerical resolution of the two-fluid Euler–Poisson model (2.1)–(2.5) presents a very restrictive constraint due to the coupling with the Poisson equation. Indeed, the Debye length λ_D must be resolved by the space discretization to guarantee the stability of the scheme (i.e. $\Delta x < \lambda_D$ where Δx is the mesh spacing). In practical situations where quasi-neutrality is established, the Debye length is very small. This implies very large computational costs in multi-dimensional cases. This is the reason why studying the quasi-neutral limit is necessary to remove the time and length scale constraints related with the electrostatic ion–electron interactions.

2.2. Formal quasi-neutral limit in the scaled Euler–Poisson model

In order to obtain the asymptotic model, we first scale the Euler–Poisson model using the device characteristic values. We denote the density scale by n_0, the ion velocity scale by u_0, the length scale by L and the applied potential difference by ϕ_0. Then, the scaled variables are defined by $\bar{n}_i = n_i/n_0$, $\bar{n}_e = n_e/n_0$, $\bar{u}_i = u_i/u_0$, $\bar{u}_e = u_e/u_0$, $\bar{x} = x/L$, $\bar{\phi} = \phi/\phi_0$, $\bar{t} = t u_0/L$, $\bar{T}_{i,e} = T_{i,e}/(m_i u_0^2)$ and $\bar{p}_{i,e} = p_{i,e}/(m_i n_0 u_0^2)$.

Introducing the scaled variables in (2.1)–(2.5) and omitting the bars gives the scaled Euler–Poisson model

$$(n_i)_t + \nabla \cdot (n_i u_i) = 0, \tag{2.7}$$

$$(n_i u_i)_t + \nabla \cdot (n_i u_i \otimes u_i) + \nabla p_i(n_i) = -n_i \nabla \phi/\eta, \tag{2.8}$$

$$(n_e)_t + \nabla \cdot (n_e u_e) = 0, \tag{2.9}$$

$$(n_e u_e)_t + \nabla \cdot (n_e u_e \otimes u_e) + \nabla p_e(n_e)/\varepsilon = n_e \nabla \phi/(\eta\varepsilon), \tag{2.10}$$

$$-\lambda \Delta \phi = n_i - n_e. \tag{2.11}$$

with

$$\varepsilon = \frac{m_e}{m_i}, \quad \eta = \frac{m_i u_0^2}{q\phi_0}, \quad \lambda = \frac{\varepsilon_0 \phi_0}{q n_0 L^2}. \tag{2.12}$$

The physical meaning of the dimensionless parameters (2.12) is the following: $\varepsilon = m_e/m_i$ is the mass ratio, η is the ratio of the thermal energy to the applied electric energy, and λ is the ratio of the applied electrical energy to the energy of coulombian interactions. In the remainder of the paper, we rescale the potential by changing ϕ into $\eta\phi$, considering that, in the plasma, the electric energy is of the order of the ion thermal energy. We obtain

$$(n_i)_t + \nabla \cdot (n_i u_i) = 0, \tag{2.13}$$

$$(n_i u_i)_t + \nabla \cdot (n_i u_i \otimes u_i) + \nabla p_i(n_i) = -n_i \nabla \phi, \tag{2.14}$$

$$(n_e)_t + \nabla \cdot (n_e u_e) = 0, \tag{2.15}$$

$$(n_e u_e)_t + \nabla \cdot (n_e u_e \otimes u_e) + \nabla p_e(n_e)/\varepsilon = n_e \nabla \phi/\varepsilon, \tag{2.16}$$

$$\lambda\eta \Delta \phi = n_i - n_e. \tag{2.17}$$

The parameter $\lambda\eta$ is related to the Debye length λ_D (2.6) by:

$$\lambda_D^2/L^2 = \lambda\eta. \tag{2.18}$$

In a quasi-neutral plasma, this parameter is very small and the limit $\lambda\eta \to 0$ is often considered.

In this limit, the solution of system (2.13)–(2.17) formally tends to the following system:

$$(n_i)_t + \nabla \cdot (n_i u_i) = 0, \tag{2.19}$$

$$(n_i u_i)_t + \nabla \cdot (n_i u_i \otimes u_i) + \nabla p_i(n_i) = -n_i \nabla \phi, \tag{2.20}$$

$$(n_e)_t + \nabla \cdot (n_e u_e) = 0, \tag{2.21}$$

$$(n_e u_e)_t + \nabla \cdot (n_e u_e \otimes u_e) + \nabla p_e(n_e)/\varepsilon = n_e \nabla \phi/\varepsilon, \tag{2.22}$$

$$n_i - n_e = 0, \tag{2.23}$$

which will be the object of our study. We note that the potential ϕ is now a sort of Lagrange multiplier of the quasi-neutrality constraint (2.23). We shall now see that this system can be written using three different but completely equivalent formulations. These formulations however cease to be equivalent at the discrete level and this paper aims at discussing the merits and drawbacks of each of them.

2.3. Three formulations of the quasi-neutral model

2.3.1. The constrained two-fluid formulation

The first formulation merely consists in keeping Eqs. (2.19)–(2.23). We may slightly transform this system in order to derive an explicit equation for ϕ. We proceed as follows: subtracting the mass conservation laws (2.19) and (2.21) and using the quasi-neutrality constraint (2.23) leads to the divergence-free equation for the current

$$\nabla \cdot (n_i u_i - n_e u_e) = 0. \tag{2.24}$$

Assuming that at the initial time $n_i = n_e$, the divergence-free constraint for the current (2.24) is equivalent to the quasi-neutrality constraint (2.23). Then, it leads to the "constrained two-fluid" formulation of the quasi-neutral model

$$(n_i)_t + \nabla \cdot (n_i u_i) = 0, \tag{2.25}$$

$$(n_i u_i)_t + \nabla \cdot (n_i u_i \otimes u_i) + \nabla p_i(n_i) = -n_i \nabla \phi, \tag{2.26}$$

$$(n_e)_t + \nabla \cdot (n_e u_e) = 0, \tag{2.27}$$

$$\varepsilon\left[(n_e u_e)_t + \nabla \cdot (n_e u_e \otimes u_e)\right] + \nabla p_e(n_e) = n_e \nabla \phi, \tag{2.28}$$

$$\nabla \cdot (n_i u_i - n_e u_e) = 0, \tag{2.29}$$

together with the following condition *on the initial data*:

$$n_i(t = 0) = n_e(t = 0). \tag{2.30}$$

Equation (2.29) allows to compute ϕ. Indeed, taking the time-derivative of (2.29) and using the momentum conservation laws (2.26) and (2.28) leads to an elliptic equation for the potential:

$$-\nabla \cdot \left[\left(n_i + \frac{n_e}{\varepsilon}\right)\nabla \phi\right] = \nabla^2 \cdot (n_i u_i \otimes u_i - n_e u_e \otimes u_e) + \Delta p_i(n_i) - \frac{\Delta p_e(n_e)}{\varepsilon}. \tag{2.31}$$

Also, we note that the operator associated with the left-hand sides of Eqs. (2.25)–(2.28) is unconditionally strictly hyperbolic, since it is constituted of two isentropic Euler operators for the electrons and the ions.

2.3.2. The 1.5-fluid formulation

We denote by $n = n_i = n_e$ the plasma density, by $j = n_i u_i - n_e u_e$ the current, and we define a new variable ψ by

$$\psi = -\left(\frac{p_i'(n)}{(\gamma_i - 1)} - \frac{p_e'(n)}{\varepsilon(\gamma_e - 1)}\right) - \left(1 + \frac{1}{\varepsilon}\right)\phi. \tag{2.32}$$

If we subtract the two momentum conservation laws (2.26) and (2.28), the constrained two-fluid formulation can be reduced to a fluid system for the variables n, u_i, j and ψ

$$n_t + \nabla \cdot (n u_i) = 0, \tag{2.33}$$

$$(1 + \varepsilon)\left[(n u_i)_t + \nabla \cdot (n u_i \otimes u_i)\right] + \nabla(p_i + p_e) = \varepsilon n \nabla \psi, \tag{2.34}$$

$$j_t + \nabla \cdot (u_i \otimes j + j \otimes u_i - j \otimes j/n) = n \nabla \psi, \tag{2.35}$$

$$\nabla \cdot j = 0. \tag{2.36}$$

We refer to this system as the "1.5-fluid formulation" because it is formulated in terms of one fluid density n and two fluid velocities or fluxes u_i and j. Therefore, it is an intermediate formulation between a fully two-fluid model like in the previous section and a fully one-fluid model like in the next section.

The new 'potential' ψ is a scalar variable which again is a sort of Lagrange multiplier of the constraint (2.36). Taking the divergence of (2.35) and using (2.36) leads to an elliptic equation for ψ:

$$-\nabla\cdot(n\nabla\psi) = -\nabla^2\cdot\left(u_i\otimes j + j\otimes u_i - \frac{j\otimes j}{n}\right). \tag{2.37}$$

The operator associated with the left-hand sides of (2.33)–(2.36) is hyperbolic but not strictly. Indeed, if we consider $d = 1$, the eigenvalues of this operator are

$$\lambda_1 = u_i - v_s, \quad \lambda_2 = u_i + v_s, \quad \lambda_3 = 2u_i - 2j/n,$$

where $v_s = ((\gamma_i T_i + \gamma_e T_e)/(1+\varepsilon))^{\frac{1}{2}}$ is the sound velocity of the plasma. If λ_3 coincide with λ_1 or λ_2, there is a resonance and the operator is not diagonalizable.

The choice of the variables n, u_i and j is a matter of physical context. One could also take n, u_e, j and keep the electron momentum conservation equation instead, or n, u and j where u is the mean velocity of the plasma $u = (u_i + \varepsilon u_e)/(1+\varepsilon)$ and keep the sum of the two momentum conservation equations.

Eq. (2.35) on j does not express a physical conservation. When shocks occur, the Rankine–Hugoniot relation for this equation is not necessarily physically true. This contrasts with the two-fluid formulation where the ion and electron momentum conservation equations express physical conservations.

2.3.3. The one-fluid formulation (for one-dimensional cases)

The 1.5-fluid formulation can be reduced to a one-fluid system. Indeed, if $n\nabla\psi$ is substituted with $j_t + \nabla\cdot(u_i\otimes j + j\otimes u_i - j\otimes j/n)$ in (2.34), we obtain

$$n_t + \nabla\cdot(nu_i) = 0, \tag{2.38}$$

$$(1+\varepsilon)\left[(nu_i)_t + \nabla\cdot(nu_i\otimes u_i)\right] + \nabla(p_i + p_e) - \varepsilon\nabla\cdot(u_i\otimes j + j\otimes u_i - j\otimes j/n) = \varepsilon j_t, \tag{2.39}$$

$$\nabla\cdot j = 0. \tag{2.40}$$

In this model, the current is no longer determined by a (constrained) time evolution equation but simply by the divergence-free constraint (2.40).

The one-fluid formulation has been intensely studied in [13–16] but it is ill-posed if the dimension d is larger than 1. Indeed, there are $2 + d$ equations for $1 + 2d$ unknowns. Following [14,15], the left-hand side of (2.38)–(2.40) is hyperbolic under the condition

$$\frac{\varepsilon}{(1+\varepsilon)^2}\frac{j^2}{n^2} < v_s^2, \tag{2.41}$$

where v_s is the above-defined plasma sound velocity.

2.3.4. Merits and drawbacks of the various formulations

In one-dimensional, and when the current j is constant in time, the right-hand side of (2.39) vanishes and the one-fluid model consists of two exact conservation laws (i.e. with no source terms). From this, we can infer that the hyperbolicity condition (2.41) gives indeed the condition for well-posedness of any of the formulations of the quasi-neutral model in a situations when the current is constant in time.

In the successive reduction from the constrained two-fluid formulation to the 1.5-fluid and one-fluid formulations, the hyperbolic part of the system passes from strictly hyperbolic to non-strictly and eventually conditionally hyperbolic. Strict hyperbolicity is a better framework for numerical simulations and we can

think that the constrained two-fluid formulation will give the best results. In fact, this conclusion is erroneous and the numerical experiments reported in the next sections show that the best formulation is 1.5-fluid one, in spite of the fact that the current conservation equation does not result from a physical conservation law. The constrained two-fluid formulation has some conditioning problems. Still, it might be useful in situations where a quasi-neutral model needs to be coupled to a non-quasi-neutral one, such as a plasma–sheath transition region. The one-fluid model is as efficient as the 1.5-fluid one [14,15] but cannot be extended in dimensions more than 1.

3. Numerical methods

3.1. General framework

To study the numerical efficiency of the various quasi-neutral formulations, we have developed appropriate numerical schemes for each formulation in the one-dimensional case.

First, let us present the general ideas of the discretization. For $x\in\Omega = [0,1]$ and $t > 0$, we write the systems (2.13)–(2.16), (2.25)–(2.28), (2.33)–(2.35) and (2.38) and (2.39) according to

$$W_t + F(W)_x = S(W), \tag{3.1}$$

where:

- For the Euler–Poisson model and the two-fluid formulation,

$$W = (n_i, n_e, n_i u_i, n_e u_e), \quad F(W) = (n_i u_i, n_e u_e, n_i u_i^2 + p_i, n_e u_e^2 + p_e/\varepsilon), \quad S(W) = (0, 0, -n_i\phi_x, n_e\phi_x/\varepsilon).$$

- For the 1.5-fluid formulation,

$$W = (n, nu_i, j), \quad F(W) = (nu_i, nu_i^2 + (p_i + p_e)/(1+\varepsilon), 2ju_i - j^2/n), \quad S(W) = (0, \varepsilon n\psi_x/(1+\varepsilon), n\psi_x).$$

- For the one-fluid formulation

$$W = (n, nu_i), \quad F(W) = (nu_i, nu_i^2 + (p_i + p_e - \varepsilon(2ju_i - j^2/n))/(1+\varepsilon)), \quad S(W) = (0, \varepsilon j_t/(1+\varepsilon)).$$

  Moreover, we consider the Poisson equation (2.17) for the Euler–Poisson system and the divergence-free current equation (2.24) for the quasi-neutral systems. Then, an initial condition $W(x,t = 0)$ is given and boundary conditions at $x = 0$ and $x = 1$ are assigned for each equation.

We define a uniform grid of size Δx on the spatial domain [0,1] with N cells $M_k =]x_{k-1/2}, x_{k+1/2}[$ $k = 1,\ldots,N$. Let Δt^n be the time step $\Delta t^n = t^{n+1} - t^n$ and let us assume that a piecewise constant approximation of the system (3.1) is given. Thus, we denote by W_k^n the approximation of W on $M_k \times [t^n, t^{n+1}[$. At each time step, the scheme consists of a time splitting: we first solve the hyperbolic part of (3.1) which gives an intermediate solution denoted by $\widetilde{W}$, and then update this solution with the source terms. Then, using a Godunov type scheme [23,55] the time-splitting scheme is given $\forall k = 1,\ldots,N$ and $n \in \mathbb{N}$ by

$$\widetilde{W}_k^{n+1} = W_k^n - \frac{\Delta t^n}{\Delta x}\left(F_{k+1/2}^n - F_{k-1/2}^n\right), \tag{3.2}$$

$$W_k^{n+1} = \widetilde{W}_k^{n+1} + \Delta t^n S(\widetilde{W}_k^{n+1}). \tag{3.3}$$

where $F_{k+1/2}^n$ is the approximate flux given by a Riemann solver.

In this paper, we use the upwind polynomial solver proposed in [17]. For the sake of completeness, we quickly recall how this solver is constructed. The numerical flux $F^n_{k+1/2}$ is an approximation of the Roe flux [23] and is defined by

$$F^n_{k+1/2} = \frac{1}{2}\left(F(W^n_k) + F(W^n_{k+1}) - \left(W^n_k - W^n_{k+1}\right)P^{k+1/2}_m\right), \tag{3.4}$$

where

$$P^{k+1/2}_m = P_m(F'(W^n_{k+1/2})) \tag{3.5}$$

is a mth degree polynomial applied to the Jacobian matrix $F'(W^n_{k+1/2})$ evaluated at the intermediate state $W^n_{k+1/2} = (W^n_k + W^n_{k+1})/2$. The polynomial $P_m(\lambda)$ is constructed to be an approximation of the absolute value function $\lambda \in \mathbb{R} \to |\lambda|$ in the interval comprised the minimal and maximal eigenvalue of $F'(W^n_{k+1/2})$. in this way, $P^{k+1/2}_m$ is an approximation of the absolute value $|F'(W^n_{k+1/2})|$ of the jacobian matrix, and (3.4) gives rise to an approximation of the Roe flux. The advantage of a polynomial expression like (3.5) is that its evaluation does not require the computation of the eigenvectors of the Jacobian matrix, by contrast with a conventional Roe scheme. In the cases where these eigenvectors are not analytically known or involve complicated algebraic function, their computation can be numerically expensive and the polynomial scheme provides an efficient and reliable approximation [17].

The polynomial P_m must satisfy certain requirement in order to ensure stability. More precisely, let $\lambda_{\max}(W)$ and $\lambda_{\min}(W)$ be the maximal and minimal eigenvalues of $F'(W)$. We define (we omit the time index n for clarity)

$$a^{k+1/2}_+ = \max\left(\lambda_{\max}\left(W_{k+1/2}\right), \lambda_{\max}(W_{k+1})\right),$$
$$a^{k+1/2}_- = \min\left(\lambda_{\min}\left(W_{k+1/2}\right), \lambda_{\min}(W_k)\right),$$

and

$$a^{k+1/2}_{\max}\begin{cases} a^{k+1/2}_+ & \text{if } |a^{k+1/2}_+| \geqslant |a^{k+1/2}_-|, \\ a^{k+1/2}_- & \text{otherwise.} \end{cases}$$

Then, according to [17], if for all $x \in [a^{k+1/2}_-, a^{k+1/2}_+]$, we have:

$$|x| \leqslant P^{k+1/2}_m(x) \leqslant |a^{k+1/2}_{\max}|,$$

the scheme (3.4) is linearly stable under the CFL condition

$$\Delta t \leqslant \frac{\Delta x}{a_{\max}} \quad \text{where } a_{\max} = \max_{k\in Z}\left(\left|a^{k+1/2}_{\max}\right|\right).$$

In the present paper, we use a second degree polynomial P_2 such that:

$$\begin{cases} P^{k+1/2}_2\left(a^{k+1/2}_+\right) = |a^{k+1/2}_+|, \\ P^{k+1/2}_2\left(a^{k+1/2}_-\right) = |a^{k+1/2}_-|, \\ P^{k+1/2}_2\left(a^{k+1/2}_{\max}\right) = \operatorname{sign}\left(a^{k+1/2}_{\max}\right). \end{cases} \tag{3.6}$$

The three constraints (3.6) define P_2 in a unique way. It should be noted that the construction of the scheme only requires the knowledge of the extreme eigenvalues, not the intermediate eigenvalues, nor the eigenvectors. This solver is first order but can easily be converted into a second order solver by using Van Leer's MUSCL procedure (see e.g. [23,55] and references therein). In the present paper, we used the unmodified first order polynomial scheme as described above.

Finally, for the Euler–Poisson model and the two-fluid formulation, we note that for the first step of the splitting (3.2), the ion and electron systems are decoupled. Then, we can consider the system (3.2) as two systems with two equations. This allows to calculate separately the ion and electron fluxes with more accuracy. Moreover, it allows to implement the Godunov scheme (see e.g. [23]).

We now investigate the computation of $S(\widetilde{W}_k^{n+1})$ for the various formulations of the quasi-neutral model.

3.2. Specific remarks pertaining to the quasi-neutral models

The divergence-free constraint (2.24) requires an additional boundary condition. In one-dimensional, this constraint reduces to $\partial_x j = 0$ or $j =$ Constant. We shall assume that this constant (generally depending on t) is known, which will be the case in the two test-problems we shall investigate later.

3.2.1. The constrained two-fluid scheme

We exploit the fact that the source terms are zero in the mass conservation equations. Then, we have $n_{i_k}^{n+1} = \widetilde{n}_{i_k}^{n+1}$ and $n_{e_k}^{n+1} = \widetilde{n}_{e_k}^{n+1}$. Since the current is constant and known at the time t^{n+1}, we have $\forall k = 1,\ldots,N$

$$j^{n+1} = (n_i u_i - n_e u_e)_k^{n+1}. \tag{3.7}$$

Then, (3.3) gives

$$(n_i u_i)_k^{n+1} = (\widetilde{n_i u_i})_k^{n+1} - \Delta t^n (n_i \phi_x)_k^{n+1}, \tag{3.8}$$

$$(n_e u_e)_k^{n+1} = (\widetilde{n_e u_e})_k^{n+1} + \Delta t^n (n_e \phi_x/\varepsilon)_k^{n+1}. \tag{3.9}$$

Combining (3.8) and (3.9) with (3.7) gives

$$(\phi_x)_k^{n+1} = -\frac{1}{\Delta t^n (n_{i_k}^{n+1} + \frac{1}{\varepsilon} n_{e_k}^{n+1})} \left[j^{n+1} - (\widetilde{n_i u_i})_k^{n+1} + (\widetilde{n_e u_e})_k^{n+1} \right]. \tag{3.10}$$

Since j^{n+1} is given, it is clear that the scheme guarantees a constant current in [0,1]. However, it does not guarantee that $n_{i_k}^{n+1} = n_{e_k}^{n+1}$ exactly but approximately (up to the order of the scheme). Then, in order to enforce the quasi-neutrality, we have investigated two possibilities. The first one consists in projecting the ion and electron densities on an average density before the computation of the electrical field $-(\phi_x)_k^{n+1}$. We call this operation the reprojection step:

$$n_{i_k}^{n+1} = n_{e_k}^{n+1} = \frac{1}{2}\left(\widetilde{n}_{i_k}^{n+1} + \widetilde{n}_{e_k}^{n+1} \right). \tag{3.11}$$

The second solution is to use a Riemann solver for the computation of the fluxes $F_{k+1/2}^n$ which guarantees the quasi-neutrality. One possibility is to use the HLLE solver and contrary to what is stated at the end of Section 3.1, to consider that the system (3.2) is a single system with four equations. We refer to Appendix A.1 for the expression of the numerical fluxes in this case. For this scheme, we can prove:

Proposition 3.1. *We consider the two-fluid formulation with HLLE fluxes as in Section A.1. We assume that quasi-neutrality holds initially, i.e. $n_i(x,t=0) = n_e(x,t=0)$ and that the current is constant, i.e. $\partial_x(n_i u_i - n_e u_e)(x,t=0) = 0$. Then, this scheme satisfies quasi-neutrality at all times exactly: $\forall k = 1,\ldots,N$ and $n \in \mathbb{N}$, we have $n_{i_k}^n = n_{e_k}^n$.*

Proof. See Section A.1. □

3.2.2. The 1.5-fluid scheme

For this formulation, the source term corresponding to the mass conservation law is zero. Then, $n_k^{n+1} = \widetilde{n}_k^{n+1}$. Since j^{n+1} is known, the equation (3.3) gives directly $(\psi_x)_k^{n+1}$ by

$$(\psi_x)_k^{n+1} = (j^{n+1} - \widetilde{j}_k^{n+1})/(n_k^{n+1}\Delta t^n). \tag{3.12}$$

3.2.3. The one-fluid scheme

For this formulation, as previously $n_k^{n+1} = \widetilde{n}_k^{n+1}$. Then, assuming that j^{n+1} is given, j_t^{n+1} is computed by:

$$j_t^{n+1} = (j^{n+1} - j^n)/\Delta t^n. \tag{3.13}$$

3.3. The Euler–Poisson scheme

For the Euler–Poisson scheme, the computation of the source terms is made in an implicit way. Indeed, we exploit the fact that the source terms are zero in the mass conservation equations. Then, $n_{i_k}^{n+1} = \widetilde{n}_{i_k}^{n+1}$ and $n_{e_k}^{n+1} = \widetilde{n}_{e_k}^{n+1}$. Since we know the densities at time t^{n+1}, the electric potential ϕ_k^{n+1} is computed by solving the Poisson equation (2.17) with Dirichlet boundary conditions using a finite difference method. We then get the electric field by approaching $-\phi_x$ by finite differences, which determines $S(W_k^{n+1})$.

4. Perturbation of a uniform plasma

This section is devoted to the study of a one-dimensional periodic perturbation about a uniform quasi-neutral stationary solution of the Euler–Poisson and quasi-neutral systems. The aim of this study is to compare the numerical solutions obtained by the various schemes (see Section 3) with the analytical solution of the linearized systems. For this purpose, we recall how to establish explicit analytical formulae for the solutions of the Euler–Poisson and quasi-neutral systems. In passing and because we need it for our numerical study, we derive the conditions for linear stability of these solutions. The proofs of the following propositions are given in Appendix A. The stability analysis of the Euler–Poisson system is classical and can be found in [5]. We note that if kinetic models are considered instead of fluid ones, more unstable regions would be found.

4.1. The linearized Euler–Poisson and quasi-neutral systems

After scaling, we consider a quasi-neutral uniform stationary solution U^0 of the Euler–Poisson system given by

$$U^0 = (n_i^0 = 1, n_e^0 = 1, u_i^0 = 0, u_e^0 = u_D, E^0 = 0),$$

where u_D is the electronic drift velocity.

4.1.1. Linear analysis of the Euler–Poisson model

In this section, we consider the Euler–Poisson system linearized about U^0.

Proposition 4.1. *Plane-wave solutions of the form* $W = \bar{W}\exp[i(kx - \omega t)]$ *of the linearized Euler–Poisson system exist iff* ω *and* k *are related by the dispersion equation*

$$\lambda\eta = \frac{1}{\omega^2 - \gamma_i T_i^0 k^2} + \frac{1}{\varepsilon(\omega - k u_D)^2 - \gamma_e T_e^0 k^2}. \tag{4.1}$$

If there exists at least one solution ω of (4.1) such that $\mathrm{Im}(\omega) < 0$, the steady state U_0 is unstable. Eq. (4.1) can be put in the form of an algebraic equation of the fourth degree and has in general four solutions which are not explicit. To solve this problem, we assume that $T_i^0 = 0$ and $k > 0$ since the dispersion relation is invariant under the transformation $(\omega,k) \to (-\omega,-k)$.

Proposition 4.2. *Assuming that $T_i^0 = 0$, we get three different configurations:*

- *If $u_D^2 > (1+\varepsilon^{-1})\gamma_e T_e^0$, then $\exists k^*$ such that the solution is unstable for $k < k^*$ and stable for $k \geqslant k^*$.*
- *If $\varepsilon^{-1}\gamma_e T_e^0 < u_D^2 < (1+\varepsilon^{-1})\gamma_e T_e^0$, then $\exists k_1,k_2$ such that the solution is unstable for $k \in]k_1,k_2[$ and stable otherwise.*
- *If $u_D^2 < \varepsilon^{-1}\gamma_e T_e^0$ then the solution is unconditionally stable.*

The thresholds $(1+\varepsilon^{-1})\gamma_e T_e^0$ and $\varepsilon^{-1}\gamma_e T_e^0$ in scaled variables correspond to the threshold values $(m_i^{-1} + m_e^{-1})\gamma_e T_e^0$ and $m_e^{-1}\gamma_e T_e^0$ in unscaled variables.

4.1.2. Linear analysis of the quasi-neutral model

In this section, we consider the quasi-neutral systems (2.25)–(2.30), (2.33)–(2.36) and (2.38)–(2.40). The linearization of these systems about U^0 leads to the same system.

Proposition 4.3. *The quasi-neutral systems (2.25)–(2.30), (2.33)–(2.36), (2.38)–(2.40) linearized about U^0 admit a plane-wave solution of the form $W = \bar{W}\exp[\mathrm{i}(kx - \omega t)]$ iff ω and k are related by the dispersion relation*

$$0 = \frac{1}{\omega^2 - \gamma_i T_i^0 k^2} + \frac{1}{\varepsilon(\omega - k u_D)^2 - \gamma_e T_e^0 k^2}. \tag{4.2}$$

The resolution of (4.2) reduces to computing the roots of a second degree polynomial function, which can be done explicitly

Proposition 4.4. *We have:*

- *If $u_D^2 > (1+\varepsilon^{-1})(\gamma_i T_i^0 + \gamma_e T_e^0)$, the solution is unstable for all k.*
- *If $u_D^2 \leqslant (1+\varepsilon^{-1})(\gamma_i T_i^0 + \gamma_e T_e^0)$, the solution is unconditionally stable.*

The threshold $(1+\varepsilon^{-1})(\gamma_i T_i^0 + \gamma_e T_e^0)$ in scaled variables correspond to the threshold value $(m_i^{-1} + m_e^{-1})(\gamma_i T_i^0 + \gamma_e T_e^0)$ in unscaled variables.

The limit $\lambda\eta \to 0$ in the Euler–Poisson dispersion equation (4.1) leads to the quasi-neutral dispersion equation (4.2). Then, in the linearized case, the solutions of the Euler–Poisson system tend to the solutions of the quasi-neutral system when $\lambda\eta \to 0$. The roots ω of (4.1) corresponding to quasi-neutral propagation modes (sound waves) tend to the roots of (4.2) when $\lambda\eta \to 0$. On another hand, the roots corresponding to plasma electron waves tend to infinity when $\lambda\eta \to 0$.

Moreover, we note that the condition of hyperbolicity (2.41) for the one-fluid formulation corresponds to the condition of linear stability for the quasi-neutral model.

4.2. Numerical simulation of a uniform plasma perturbation

4.2.1. Parameters of the numerical simulation

We select parameters issued from plasma arc physics (see e.g. [6,19,39]) that lead to the following values: $\gamma_i = \gamma_e = 5/3$, $c_i = c_e = 1$, $\varepsilon \sim 10^{-4}$, $\sqrt{\lambda\eta} \sim 10^{-3}$, $u_D = 1$. The perturbation is taken monochromatic with a wave number k equal to 2π, and the perturbation at initial time is set to $n_i^1(t=0) = n_e^1(t=0) = 0$, $u_i^1(t=0) = u_e^1(t=0) = 10^{-2}$.

We note that the scaled values of the electron plasma frequency ω_p and of the sound velocity v_s are

$$\omega_p = \frac{1}{\sqrt{\varepsilon\lambda\eta}} = 10^5, \quad v_s = \left(\frac{\gamma_i T_i^0 + \gamma_e T_e^0}{1+\varepsilon}\right)^{\frac{1}{2}} = 11.47. \tag{4.3}$$

The values $\pm\omega_p$ and $\pm k\, v_s$ correspond to the roots ω of the Euler–Poisson dispersion relation calculated by a QR method [32]. These roots are real numbers which corresponds to a stable regime. We notice that the high frequency modes correspond to the plasma frequency and the low frequency modes to the sound waves in the plasma.

The roots of the linearized quasi-neutral system are directly obtained by solving the dispersion equation (4.2) which leads to $\omega \simeq \pm k v_s = 11.47$ and corresponds to a stable case. Furthermore, high frequency modes of the Euler–Poisson model which are associated with plasma waves have disappeared in the quasi-neutral limit while low frequency acoustic waves remain. We can see that the quasi-neutral limit leads to a drastic reduction of the stiffness of the problem.

4.2.2. Accuracy of the different schemes

We study the accuracy of the schemes given in Section 3. For all the systems, the reference solution is the linearized Euler–Poisson analytical solution. We define the relative error on the ion and electron densities at time t^n as

$$\delta n_{i,e} = \frac{||n_{i,e}^n - n_{i,e}^*(x,t^n)||_{l_2}}{||n_{i,e}^n - n^0||_{l_2}} = \left[\frac{\sum_{k=1}^{N}\left((n_{i,e})_k^n - n_{i,e}^*(x_k,t^n)\right)^2}{\sum_{k=1}^{N}\left((n_{i,e})_k^n - 1\right)^2}\right]^{\frac{1}{2}}, \tag{4.4}$$

where $n_{i,e}^*$ is the analytical density of the Euler–Poisson model linearized about U^0 and $x_k = (k + 1/2)\Delta x$ for all $k = 1$ to N.

First, we study the constrained two-fluid scheme. We compare the polynomial scheme without reprojection method, the polynomial scheme with reprojection method and the HLLE scheme (which does not need any reprojection step since it ensures $n_e = n_i$ automatically). In Fig. 1, the ion density (left figure) and electron density (right figure) obtained at a fixed time ($t = 0.12$) by these three schemes are compared with the analytical solution of the linearized Euler–Poisson system for different values of the mesh size Δx. First, we observe that all schemes converge towards the analytical solution when $\Delta x \to 0$. Then, we note that even if it guarantees quasi-neutrality, the HLLE scheme remains of low accuracy compared with a polynomial scheme. Moreover, for the polynomial scheme, the reprojection step degrades the accuracy for the ion density but improves it for the electron density. In the remainder of this work, we shall use the polynomial scheme with reprojection step for the implementation of the constrained two-fluid scheme.

Then, we compare the accuracy of the constrained two-fluid, 1.5-fluid, one-fluid and Euler–Poisson schemes. The schemes are all implemented with a polynomial solver.

In Fig. 2 (left figure), we plot δn_i as a function of Δx at a fixed time ($t = 0.12$). We first observe that the error decreases when the mesh size Δx decreases but eventually saturates to a finite value. Indeed, the error

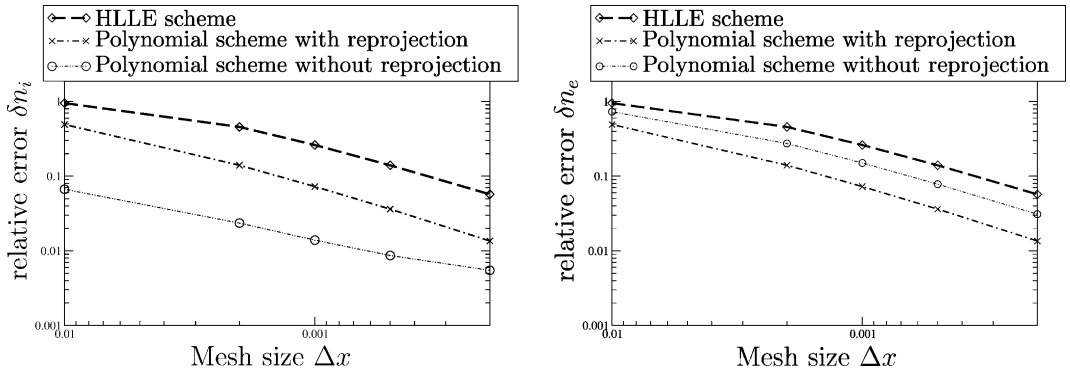

Fig. 1. Relative error on the ion density (left) and on the electron density (right) at a fixed time ($t = 0.12$) as a function of the mesh size Δx for three schemes solving the constrained two-fluid model: the HLLE scheme (dashed line), the polynomial scheme without reprojection step (dotted line) and the polynomial solver with reprojection step (dashed-dotted line). The HLLE scheme preserves quasi-neutrality. The polynomial scheme does not and quasi-neutrality can be enforced using (3.11) (reprojection step) or not.

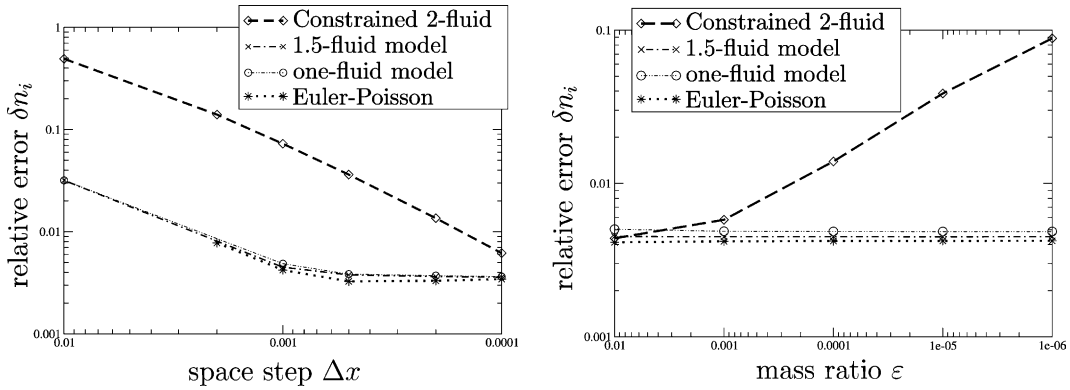

Fig. 2. Relative error on the ion density at a fixed time ($t = 0.12$), as a function of the mesh size (left) and as a function of the mass ratio ε for a fixed mesh size $\Delta x = 10^{-3}$ (right). The constrained two-fluid scheme has a poorer convergence as $\Delta x \to 0$ than the two- and 1.5-fluid models and its accuracy depends on the mass ratio ε while the other ones do not.

is computed by comparison with the analytical solution of the linearized model, while the schemes actually converge to that of the non-linear model. This saturation reflects the difference between the solution of the linearized and non-linear models. Nonetheless, we can use these results before saturation to study the numerical efficiency of the different schemes. We observe that the order of convergence is $O(\Delta x)$ for all the schemes and we observe that the 1.5-fluid, one-fluid and Euler–Poisson schemes are more accurate than the constrained two-fluid scheme.

In Fig. 2 (right figure), we plot δn_i as a function of ε at time $t = 0.12$ with $\Delta x = 10^{-3}$. We observe that the accuracy of all the numerical schemes is independent of the mass ratio ε but for the constrained two-fluid scheme, whose accuracy degrades as $\varepsilon \to 0$.

Then, evaluating graphically the orders of convergence leads to the following conclusions:

- The order of convergence of the one-fluid, 1.5-fluid and Euler–Poisson schemes is $O(\Delta x)$.
- The order of convergence of the constrained two-fluid scheme is $O(\Delta x/\sqrt{\varepsilon})$.

Similar observations made on the ion and electron velocities have confirmed these conclusions.

We can draw a certain number of conclusions from this analysis. First of all, the constrained two-fluid formulation appears to be less efficient than the 1.5- and one-fluid formulations. At first glance, one could think that the inefficiency of the constrained two-fluid formulation is linked to the fact that the electron and ion densities have to be made equal by some artificial numerical procedure. However, this conclusion is erroneous since the HLLE scheme which does not require any reprojection step according to Proposition 3.1 appears to be of lower accuracy than a polynomial scheme which does need such a reprojection procedure (see Fig. 1).

Second, the loss of accuracy of the constrained two-fluid formulation appears to be related to the fact that ε multiplies the time derivative in the momentum equation (2.28), i.e. to an ill-conditioning of this equation. In the other formulations, ε never multiplies the time derivatives alone (only the factor $(1+\varepsilon)$ does) and this conditioning problem does not appear. This conclusion is supported by the numerical determination of the orders of accuracy, which is ε-dependent for the constrained two-fluid model but ε-independent for the 1.5- and one-fluid models.

5. Plasma expansion in vacuum

We are interested in a one-dimensional modeling of a quasi-neutral plasma expansion in vacuum between two electrodes. The plasma is injected at the cathode and undergoes a thermal expansion. At the front of the plasma, electrons are attracted by the positive potential of the anode and are emitted. The emission creates an electron beam in the vacuum from the plasma front to the anode, and this process generates a current in the whole device and in particular in the plasma.

This phenomenon is studied in relation with two physical applications: high-current diodes [30,34,45,54,57], and arcing on satellite solar generators [6,19,25–28,38,39,50,51,56]. A series of works [13–16] have been realized to describe this process. In all these works, the plasma is described by the one-fluid formulation of the quasi-neutral model. The electron beam is described by an analytical Child–Langmuir model (see e.g. [5,11,12,18]). Finally, a transmission problem is resolved to couple the plasma and the beam models.

We first summarize the model proposed in [14,15]. In Section 5.2, we describe the numerical methods used for interface tracking. Finally, in Section 5.3, we present the numerical results.

5.1. Models for the plasma and beam regions, transition problem

We refer to Section 2.2 for the scaling. In scaled variables, the cathode is located at $x = 0$, the anode at $x = 1$ and a potential difference $\phi_L = \eta^{-1}$ is applied between these two electrodes. A quasi-neutral plasma is injected at the cathode such that $n_i|_{x=0} = n_e|_{x=0} = 1$, $u_i|_{x=0} = 1$, and $u_e|_{x=0} = 1$. Setting the potential origin at $x = 0$ gives $\phi|_{x=0} = 0$ and $\phi|_{x=1} = \phi_L$. At the initial time $t = 0$, the domain is free of plasma.

At time $t = 0$, the electrons and the ions penetrate the domain. We denote by $X_e(t)$ and $X_i(t)$ the positions of the electron–vacuum and ion–vacuum interfaces. Because of the acceleration of the electrons by the potential, $X_e(t)$ reaches the anode $x = 1$ after a very short time while $X_i(t)$ proceeds more slowly. Formally, $X_i(t) \to X(t)$ when $\lambda\eta \to 0$, where $X(t)$ is the interface between the quasi-neutral plasma region and the region where the electrons are accelerated (the beam region). Therefore, the quasi-neutral region $[0, X(t)[$ can be described by one of the formulations of the quasi-neutral model. The region $[X(t), 1]$ is occupied by the electron beam and is devoid of ions, and, according to [14,15], can be described by the Child–Langmuir model [18,31]. This is a stationary model: the electrons being accelerated by the very strong electric potential, of order η^{-1}, cross the gap almost instantaneously. The current is given by the Child–Langmuir relation, which, in our scaled units, reads:

$$-n_e u_e(x,t) = j_{CL}(t) = -4\frac{\sqrt{2}\lambda}{9}\frac{1}{(1-X(t))^2\sqrt{\eta\varepsilon}}. \tag{5.1}$$

The electron density and electric potentials have analytical formulations (see [14,15,18,31]).

The connection between the quasi-neutral plasma model and the Child–Langmuir model for the beam is realized through the following matching conditions:

- the velocity of the interface is such that
$$dX/dt = u_i(X(t),t) \quad \forall t > 0, \tag{5.2}$$
- the current is continuous across the interface
$$j(t) = n_i u_i(x,t) - n_e u_e(x,t) = j_{CL}(t) \quad \forall x \in [0,1],\ \forall t > 0, \tag{5.3}$$
- a range of admissible values are given for the quasi-neutral density at the interface
$$n_i(X(t),t) = n_e(X(t),t) \leqslant n_p(t), \tag{5.4}$$
where n_p is determined by
$$\gamma_i c_i n_p^{\gamma_i+1} + \gamma_e c_e n_p^{\gamma_e+1} = \varepsilon j^2.$$
- The electric potential at the interface vanishes:
$$\phi(X(t),t) = 0. \tag{5.5}$$

Condition (5.2) states that the plasma–beam interface is the boundary of the region occupied by the ions, since the electrons fill the whole gap (see the discussion at the beginning of this section). This boundary obviously moves with the velocity of the ions at this boundary, which is what (5.2) expresses. The second condition (5.3) matches the plasma current (described by the quasi-neutral model) with the beam current (described by the Child–Langmuir law). It assumes that charge variations in the transition region are negligible. Condition (5.4) means that the plasma is supersonic with respect to the interface velocity, which is a possible formulation of Bohm's sheath criterion (see e.g. [42]). Finally, (5.5) expresses that the potential being continuous and identically zero in the plasma quasi-neutral region, must be equal to zero at the interface. All four conditions have been justified by an analytical study of the transition region in [15].

We stress the fact that we do not impose any condition on the electron density at the interface $X(t)$ on the beam side. Indeed, the electron density obtained through the Child–Langmuir law is given by $n_e = j_{CL}/\sqrt{\phi}$ (see e.g. [18,31]) and is infinite since $\phi(X) = 0$. As a result, the description of the transition region by this asymptotic model is not very accurate, since the actual electron density (as given by the Euler–Poisson models for instance) remains finite. However, the transition region is very tiny and there is a fairly good agreement between the original Euler–Poisson model and the asymptotic model away from the transition region as we shall see further on the numerical results.

5.2. Numerical methods, interface tracking

In this section, we complete the description of the numerical schemes for the plasma expansion problem. We recall that the quasi-neutral model is defined only on the plasma domain $[0,X(t)[$. The main difficulties here are the interface localization, the description of its motion and the computation of the fluxes across it.

According to [14,15], we choose a front tracking method to localize the interface, which is the most natural method for one-dimensional simulations. Eq. (5.2) can be discretized by an Euler scheme

$$X^{n+1} = X^n + \Delta t^n u^n_{i_X}, \tag{5.6}$$

where $u^n_{i_X}$ is an approximation of $u_i(X(t^n),t^n)$ and is determined below. Thanks to (5.1), (5.3) and (5.6), the current at time t^{n+1} can be computed as soon as the position X^n and the velocity $u^n_{i_X}$ of the interface at time t^n are known.

For the computation of the first step of the time splitting (see Section 3), we assume that the right-end of the last cell corresponds to the plasma–beam interface. To this aim, we denote by k_0 the index such that $X^n \in]x_{k_0-\frac{1}{2}}, x_{k_0+\frac{1}{2}}[$, and we define an adaptive space discretization. At time t^n, we have

$$M_k =]x_{k-\frac{1}{2}}, x_{k+\frac{1}{2}}[\quad \forall k \leqslant k_0 - 2 \quad \text{and} \quad M_{k_0-1} =]x_{k_0-\frac{3}{2}}, X^n[. \tag{5.7}$$

In Fig. 3, we represent the trapezoidal rightmost space–time cell of the mesh. The numerical scheme for the space–time cells $M^n_k \times [t^n, t^{n+1}]$ has already been given in Section 3 when $k < k_0-1$. The scheme on the last cell is given by

$$(X^{n+1} - x_{k_0-\frac{3}{2}})\widetilde{W}^{n+1}_{k_0-1} - (X^n - x_{k_0-\frac{3}{2}})W^n_{k_0-1} + \Delta t^n \left(F^n_{k_0-\frac{1}{2}} - F^n_{k_0-\frac{3}{2}}\right) = 0, \tag{5.8}$$

where $F^n_{k_0-\frac{3}{2}}$ is classically given by a Riemann solver and $F^n_{k_0-\frac{1}{2}}$ is given by

$$F^n_{k_0-\frac{1}{2}} = -W^n_v u^n_{i_X} + F(W^n_v), \tag{5.9}$$

where W^n_v is the solution at the interface.

For the one-fluid scheme, the state $W^n_v = (n, nu_i)^n_v$ is computed by resolving a Riemann problem where the left state is the plasma state $W^n_{k_0-1}$ before the interface and the right state is the vacuum. The condition (5.4) is taken into account as follows. If $n^n_{k_0-1} \leqslant n_p(t^n)$ then the solution of the Riemann problem at the interface is the plasma state $W^n_{k_0-1}$ separated from the vacuum by a shock wave moving with the speed $(u_i)^n_{k_0-1}$. Else, the solution of the Riemann problem involves a rarefaction wave associated with the first characteristic field connecting $n^n_{k_0-1}$ to $n_p(t^n)$. This leads to $(n_i)_v = n_p$ and to the determination of $(u_i)^n_v$ (see [14,15] for the details).

For the 1.5-fluid scheme, we have $W^n_v = (n, nu_i, j)^n_v$. At the interface, $(n, u_i)^n_v$ is given as previously and the current j^n_v is given following (5.3), i.e. $j^n_v = j^n$. Finally, in the two-fluid case, the state of ions at interface $(n_i, n_i u_i)^n_v$ is still given as previously. Then, considering that the plasma is quasi-neutral at the interface, and following (5.3) we have $n^n_{e_v} = n^n_{i_v}$ and $u^n_{e_v} = u^n_{i_v} - j^n/n^n_{i_v}$. The interface velocity is given by the state of ions at the interface such that $u^n_{i_X} = (u_i)^n_v$.

5.3. Numerical results

We study a case of arcing on satellite generators [6,19,39]. The physical values for this problem are $\gamma_i = \gamma_e = 5/3$, $c_i = c_e = 1$, $\varepsilon \sim 10^{-4}$, $\lambda \sim 10^{-4}$ and $\eta \sim 10^{-2}$. The Euler–Poisson results are given as a reference.

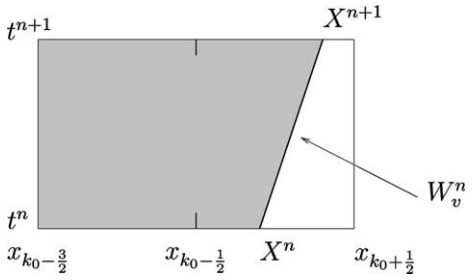

Fig. 3. Rightmost space–time cell of the mesh before the interface.

We first discuss the results of the constrained two-fluid scheme at the scaled times $t = 0.05$ and $t = 0.15$. In Fig. 4 (top), we represent the ion density (top left) and electron density (top right) as functions of x, obtained by the constrained two-fluid model implemented with a polynomial solver without reprojection step. We observe that the ion density is fairly well approximated and that the interface is well localized. However, there is a large error on the electron density and the results are far from quasi-neutrality. In Fig. 4 (bottom left) we represent the density obtained by the same scheme together with a reprojection step (electron and ion densities being forced to be equal, there is only one single figure). In this case, the quasi-neutrality is enforced but the error remains very large and the interface is badly localized. In Fig. 4 (bottom right) we show the same results computed on a refined mesh (Δx has been divided by 4). We observe that the results have improved. Yet, the convergence of the constrained two-fluid scheme when $\Delta x \to 0$ appears again to be quite slow. This confirms the observations made in Section 4.2.2 about the ill conditioning of the constrained-two fluid model.

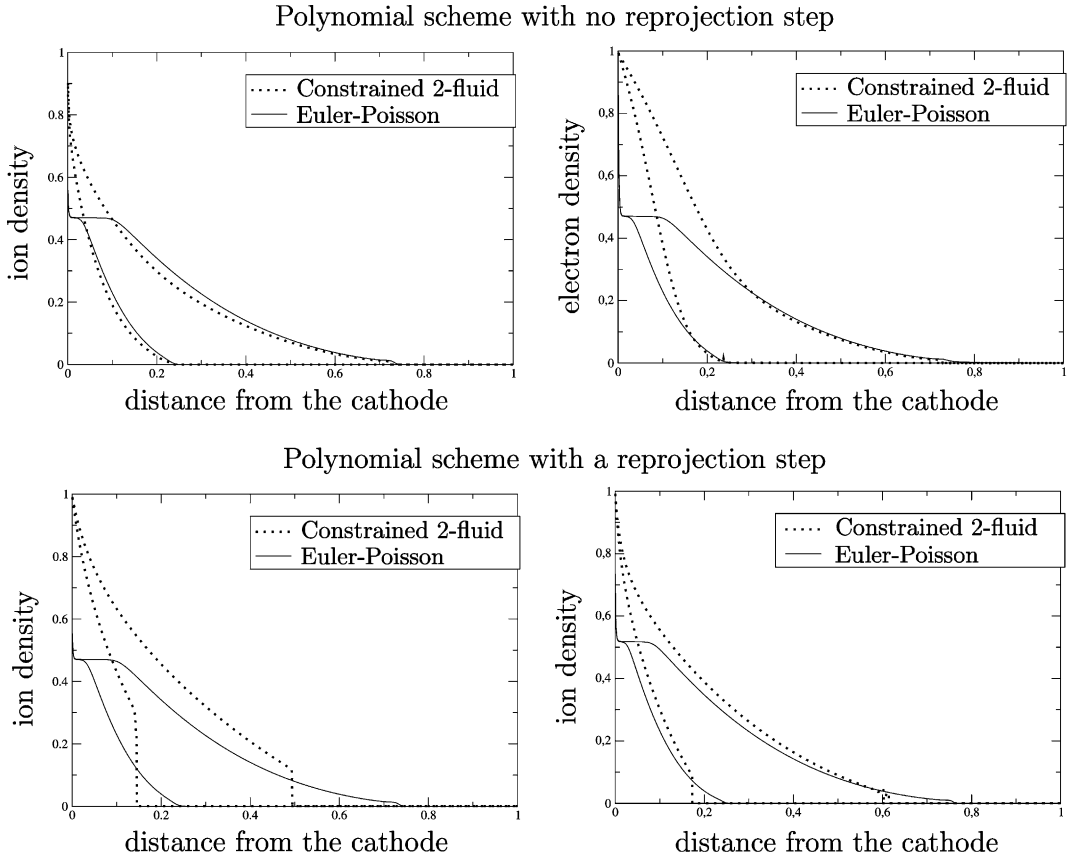

Fig. 4. Constrained two-fluid model. Top figures: without reprojection step enforcing quasi-neutrality, the ion density (top left) and electron density (top right) are away from each other. They are plotted as functions of x at times $t = 0.05$ and $t = 0.15$ for $\Delta x = 10^{-3}$. Bottom figures: with reprojection step, the electron and ion densities are forced to be equal. They are plotted as functions of x at times $t = 0.05$ and $t = 0.15$ for $\Delta x = 10^{-3}$ (left) and $\Delta x = 2.5 \times 10^{-4}$ (right). All these results are compared with the Euler–Poisson model computed on a mesh with $\Delta x = 5 \times 10^{-4}$.

Then, we discuss the results of the 1.5-fluid model. In Fig. 5, we represent the quasi-neutral density (top left figure), the ion velocity (top right figure) and the electron velocity (bottom figure) as functions of x in the plasma zone at times $t = 0.05$ and $t = 0.15$. We observe that the 1.5-fluid model behaves globally quite well within the plasma region. There are two zones where a significant discrepancy occurs: the transition region between the plasma and the beam regions on the one-hand and the injection zone located near the cathode where a boundary layer seems to form. We successively focus on these two regions to better understand the reasons of these discrepancies.

In Fig. 6, we magnify the interface zone at the scaled time $t = 0.15$. In the top figure, we represent the ion and electron densities given by the Euler–Poisson model as functions of x in the interface region and compare them with the quasi-neutral density obtained by the 1.5-fluid scheme. In the bottom figure, the ion velocities obtained by the Euler–Poisson and 1.5-fluid schemes are represented as functions of x. According to the Euler–Poisson results, we observe that we have a smooth transition from the quasi-neutral plasma to the electron beam. The transition region represents about 4–5% of the domain. In this region, the ion density and velocity decrease smoothly from a non-zero value to zero, while the electron density remains nearly constant. With the 1.5-fluid model, this transition is replaced by jump discontinuities of the quasi-neutral density and ion velocity from a non-zero value in the plasma to zero in the beam. This behavior is a direct consequence of the matching condition (5.4), which allows the existence of an interface shock (see also the

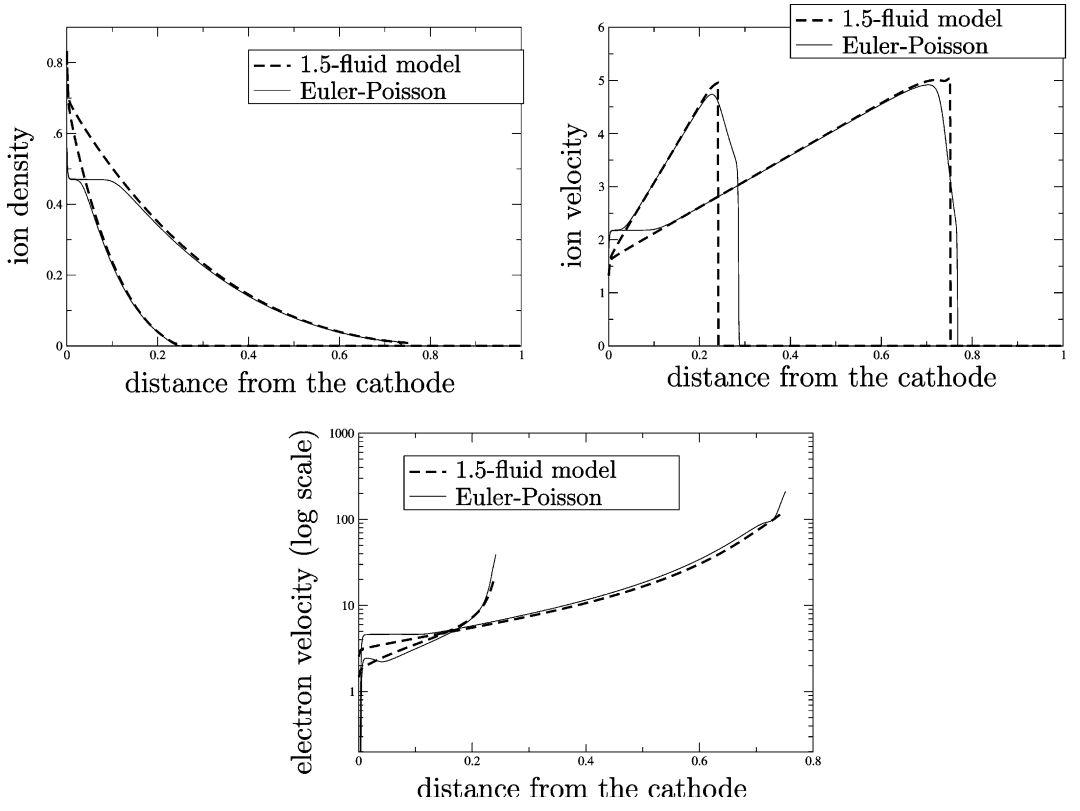

Fig. 5. 1.5-fluid model: quasi-neutral density (top left figure), ion velocity (top right figure) and electron velocity (bottom figure) as functions of x at times $t = 0.05$ and $t = 0.15$ with $\Delta x = 10^{-3}$. The simulations are compared with the results of the Euler–Poisson scheme with mesh size $\Delta x = 5 \times 10^{-4}$.

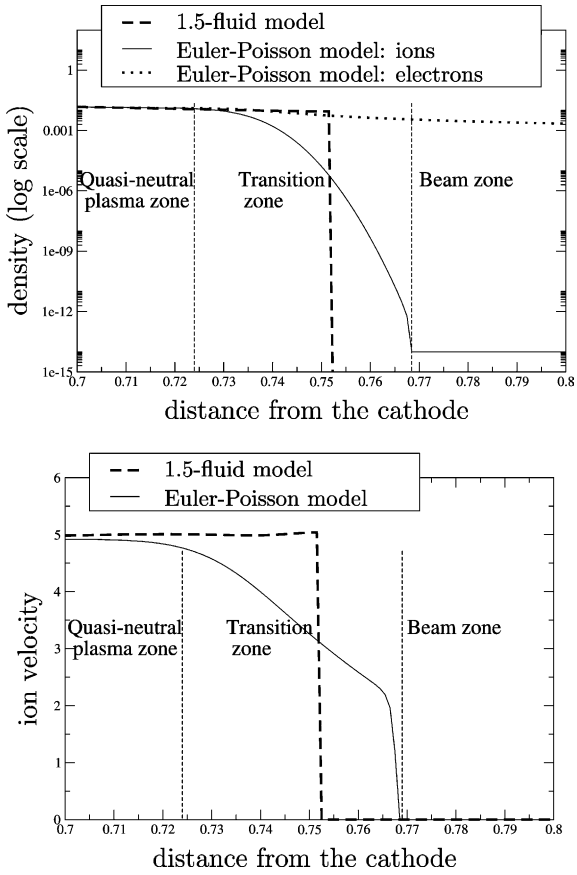

Fig. 6. 1.5-fluid model: magnification of the densities (top) and ion velocity (bottom) as functions of x in the vicinity of the plasma–beam interface at time $t = 0.15$. In the top figure, the 1.5-fluid quasi-neutral density (dashed line) is compared with the electron density (dotted line) and ion density (solid line) obtained by the Euler–Poisson model. In the bottom figure, the 1.5-fluid ion velocity (dashed line) is compared with the Euler–Poisson ion velocity (solid line). In both figures, the boundaries of the transition zone are indicated by two vertical dotted lines.

discussion at the end of Section 5.2). In this figure, for the sake of clarity, we have not displayed the electron density in the beam region as given by the Child–Langmuir law. If we had done so, we would see that this density is infinite on the right of the interface shock, and would then decrease smoothly and rejoin the density given by the Euler–Poisson scheme (see also Fig. 9 and its discussion below). It should be noted however that the position of the interface shock is correctly determined by the 1.5-fluid scheme as it remains within the transition zone. This is important to obtain a good agreement in the beam region, since the Child–Langmuir current (5.1) is directly related to the position of the interface.

In Fig. 7, we magnify the region close to the cathode (which we refer to as the 'injection zone') at the scaled time $t = 0.15$. We represent the densities (top left figure), the ion velocity (top right figure) and the current (bottom figure) obtained by the 1.5-fluid and Euler–Poisson models as functions of x. The Euler–Poisson simulations show that a non-quasi-neutral boundary layer prevails in the injection region and the quasi-neutral model is not well suited to this region. However, it is noticeable that the values of the density and ion velocity obtained by the Euler–Poisson model at the right-end of the injection region

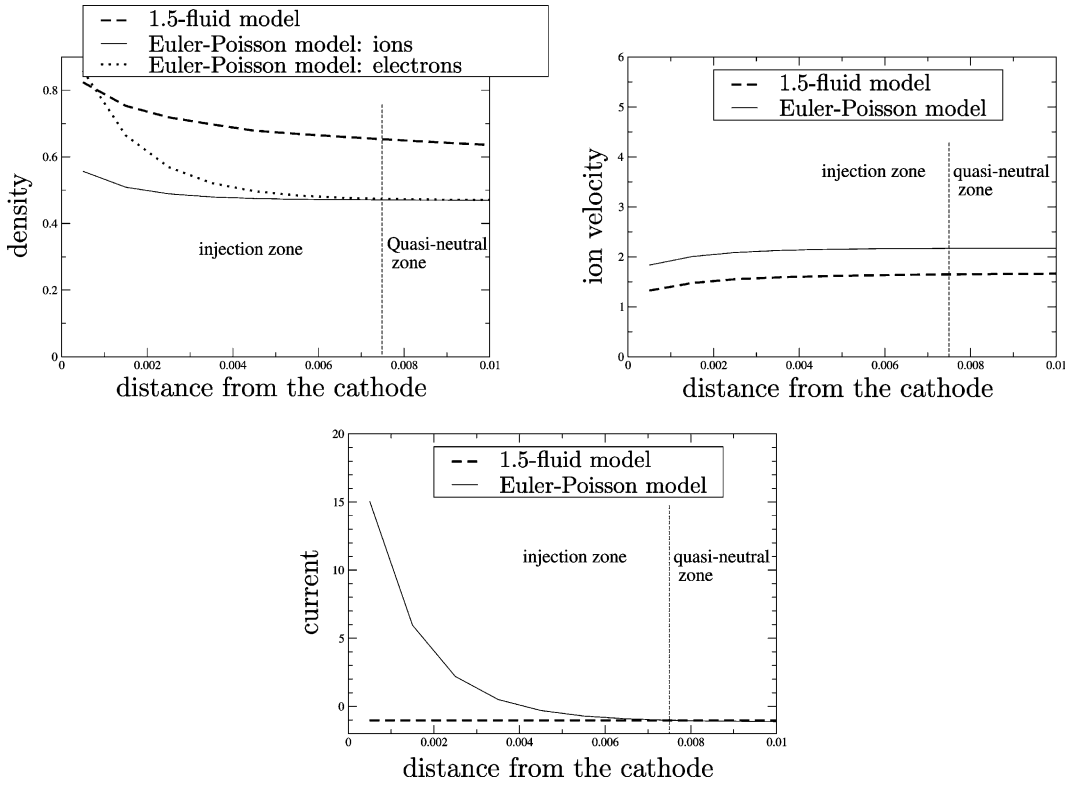

Fig. 7. 1.5-fluid model: magnification of the densities (top left), ion velocity (top right), and current (bottom) as functions of x in the vicinity of the cathode (injection zone) at time $t = 0.15$. In the top left figure, the 1.5-fluid quasi-neutral density (dashed line) is compared with the electron density (dotted line) and ion density (solid line) obtained by the Euler–Poisson model. In the top right figure, the 1.5-fluid ion velocity (dashed line) is compared with the Euler–Poisson ion velocity (solid line). In the bottom figure, the uniform electrical current of the quasi-neutral model is compared with the non-uniform current obtained by the Euler–Poisson model. The mesh size is $\Delta x = 10^{-3}$ for the 1.5 fluid model and $\Delta x = 5 \times 10^{-4}$ for the Euler–Poisson model. The boundary of the injection zone has been indicated by a vertical dotted line.

remain nearly constant in time. If these values are used as boundary conditions for the 1.5-fluid model the results improve dramatically, as shown in Fig. 8. We represent the ion and quasi-neutral densities (top left figure), the ion velocity (top right figure) and the electron velocity (bottom figure) in the plasma zone at the scaled times $t = 0.05$ and $t = 0.15$, and observe that there is a good agreement between the 1.5-fluid model and the Euler–Poisson model. This indicates that a boundary layer model is necessary to correctly prescribe the boundary values of the quasi-neutral model on the cathode side. The derivation of such a boundary layer model is work in progress.

In Fig. 9, we study the Child–Langmuir law approximation for the beam region at the scaled times $t = 0.05$ and $t = 0.15$. We represent the electron density (top left figure), the electric potential (top right figure), the electron velocity (bottom left figure) as functions of x in the beam region. In the bottom right figure, the current is shown as a function of x in the whole device. We observe that the Child–Langmuir law approximation is rather well suited to the description of the beam and to the computation of the current in the plasma. The small errors than can be observed seem to be related to the approximation of the location of the plasma–beam interface.

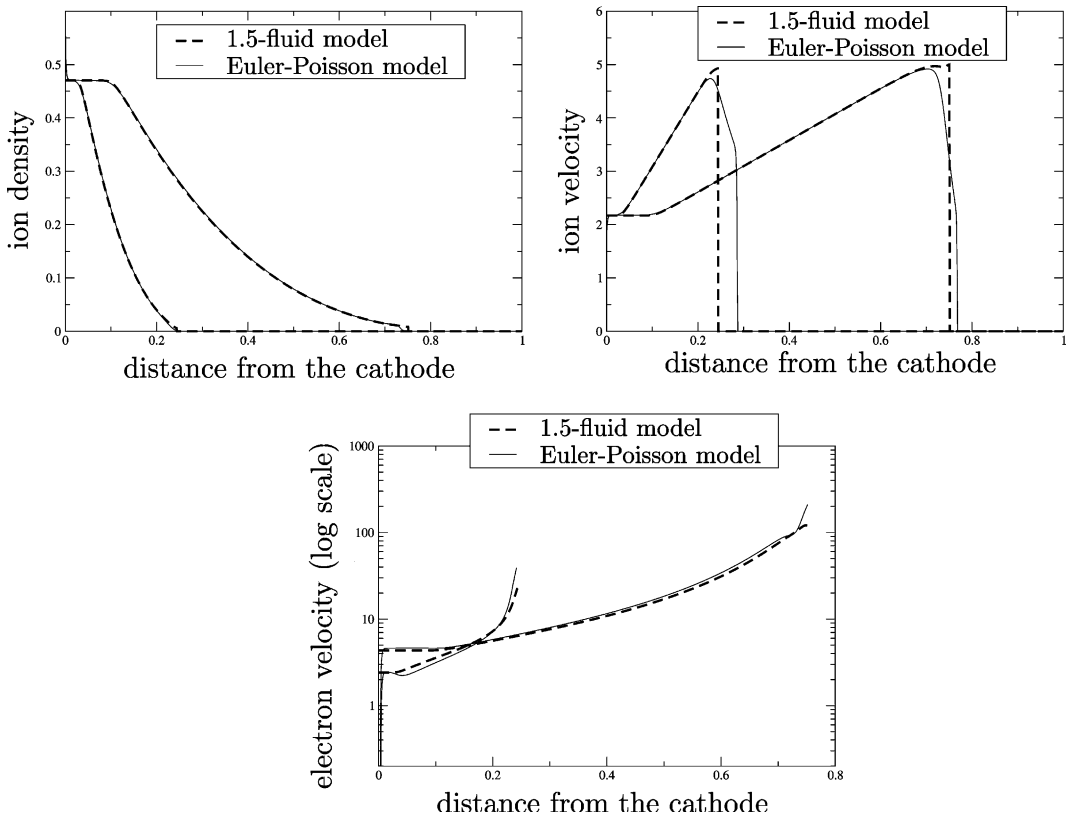

Fig. 8. 1.5-fluid model: the boundary conditions for the 1.5-fluid model at $x = 0$ have been set equal to the values computed from the Euler–Poisson model at the right-end of the injection zone (see Fig. 7). In the top left figure, the 1.5-fluid quasi-neutral density is compared with the ion density of the Euler–Poisson model. Ion velocities and electron velocities are displayed on the top right figure and bottom figure, respectively. The figures have been taken at time $t = 0.05$ and $t = 0.15$. The mesh size is $\Delta x = 10^{-3}$ for the 1.5 fluid model and $\Delta x = 5 \times 10^{-4}$ for the Euler–Poisson model. We can observe a good agreement between the two models over the plasma region.

Results from the one-fluid model are not shown in this section because the results are very similar to those of the 1.5-fluid model. However, the one-fluid model breaks down earlier because the hyperbolicity condition is violated.

Finally, oscillations occur at the plasma–vacuum interface for the 1.5-fluid and two-fluid models, and lead to the breakdown of the simulations. It appears that these oscillations depend on the mesh refinement but they happen earlier in time when the mesh is refined. On the same way, the condition of hyperbolicity of the one-fluid scheme is violated earlier when the mesh size decreases. The density (left figure) and ion velocity (right figure) obtained by the 1.5-fluid model at time $t = 0.10$ and for $\Delta x = 10^{-4}$ are plotted in Fig. 10. We can observe the development of these oscillations near the plasma–beam interface. Moreover, in Table 1, we list the times corresponding to the breakdown of the 1.5-fluid and one-fluid schemes as functions of the mesh size.

The breakdown of the various schemes can be attributed to a physical two-stream instability which occurs when the plasma current reaches large values as the interface moves closer to the anode. In these conditions, non-quasi-neutral modes may be excited, which the quasi-neutral model fails to describe. As a

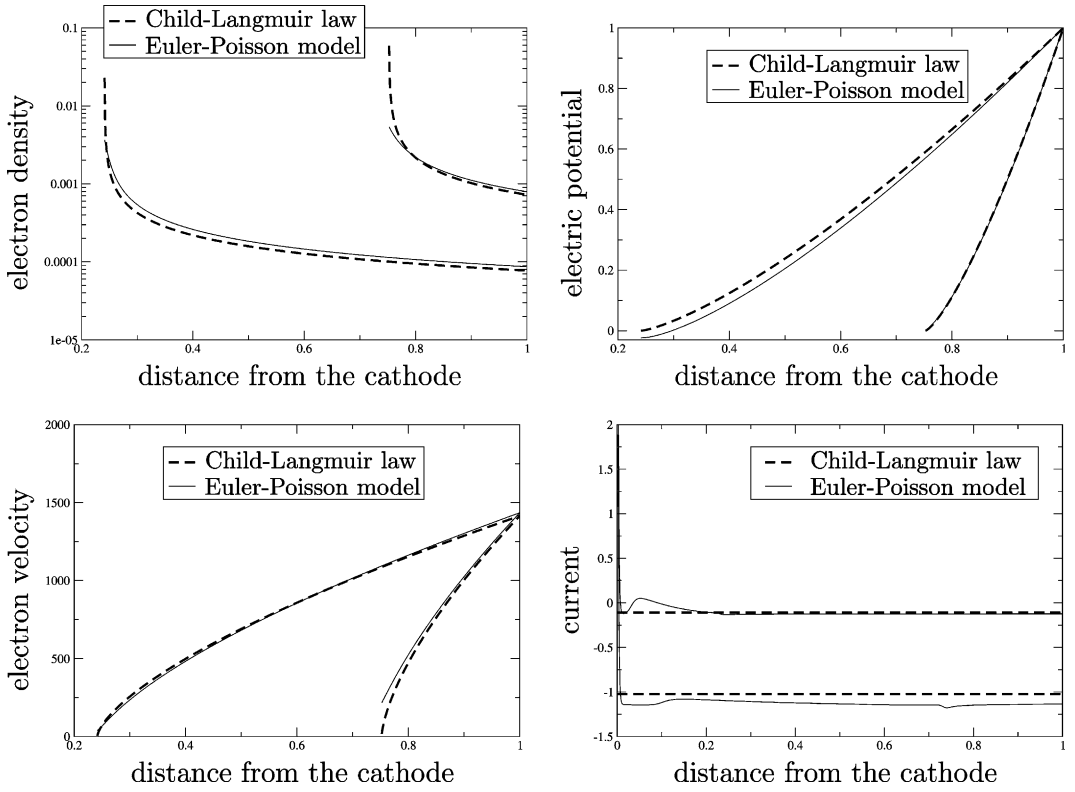

Fig. 9. Child–Langmuir law in the beam region: comparison with the Euler–Poisson model. Electron density (top left figure), electric potential (top right figure), electron velocity (bottom left figure) and current (bottom right figure) as functions of x at times $t = 0.05$ and $t = 0.15$. The mesh size is $\Delta x = 5 \times 10^{-4}$ for the Euler–Poisson model. The Child–Langmuir solution is computed analytically, following [15,18,31]. We observe a good agreement between the two models. The singularity of the Child–Langmuir density at the interface can be noticed.

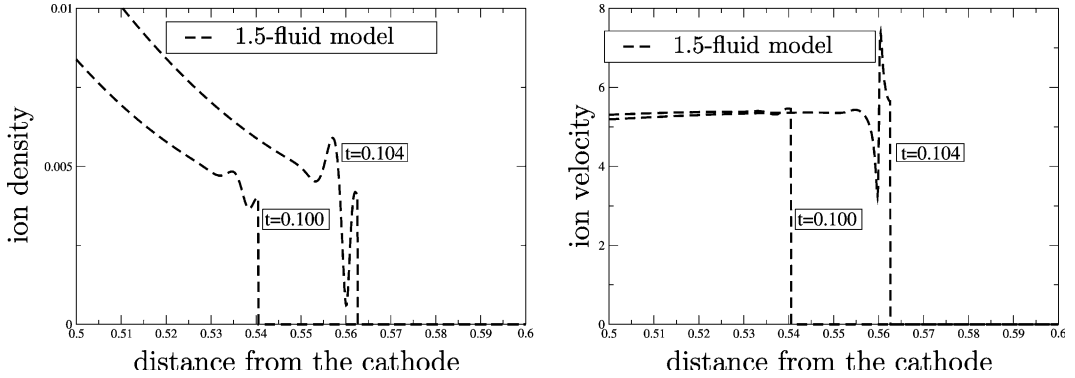

Fig. 10. Breakdown of the 1.5-fluid model: ion density (left) and ion velocity (right) as functions of x at the scaled times $t = 0.100$ and $t = 0.104$. Oscillations start to develop at the interface, eventually leading to a negative density. The mesh size is $\Delta x = 10^{-4}$.

Table 1
Scaled times t_{max} corresponding to the breakdown of the one-fluid and 1.5-fluid schemes as functions of the mesh size

	One-fluid model	1.5-Fluid model
$\Delta x = 10^{-3}$	$t_{max} \sim 0.08$	$t_{max} \sim 0.17$
$\Delta x = 2 \times 10^{-4}$	$t_{max} \sim 0.04$	$t_{max} \sim 0.12$
$\Delta x = 10^{-4}$	$t_{max} \sim 0.03$	$t_{max} \sim 0.10$
$\Delta x = 5 \times 10^{-5}$	$t_{max} \sim 0.02$	$t_{max} \sim 0.09$

result, a numerical instability develops and leads to the collapse of the numerical scheme. Moreover, with a smaller mesh size, the numerical diffusion is lower and offers a weaker resistance against the instability, thus explaining that breakdown occurs earlier. It is therefore desirable to develop a model which allows non-quasi-neutral modes to develop in such extreme situations. The derivation of such a model is the subject of current research.

6. Conclusion

In this paper, we have proposed three formulations of a quasi-neutral model with a non-vanishing current. We have implemented the various formulations on two test-problems and compared their numerical efficiencies. Moreover, we have developed a linear analysis of the quasi-neutral model.

The conclusions of this study are that, on the one hand, the 1.5-fluid model seems the most efficient model for the numerical modeling of a current-carrying quasi-neutral plasma. Indeed, the two-fluid model has a lower accuracy related to the mass ratio of the species in the plasma, and the one-fluid model can only be used in one-dimensional cases. On the other hand, it would be desirable for the quasi-neutral model to be easily connected with non-quasi-neutral regions (such as sheath regions). From this point of view, the constrained two-fluid formulation seems to be best adapted for this coupling. Using this idea, a hybrid model which allows a smooth transition from the constrained two-fluid formulation of the quasi-neutral model to the Euler–Poisson model is currently under development.

Of course, realistic applications of the present study (such as high-current diodes, arcing on solar cells or more generally, plasma–sheath problems) are intrinsically two- or three-dimensional. In practice, multi-dimensional interface problems require a complicated and expensive interface tracking procedure unless some smoothing of the interface is performed, in the spirit of level-set methods for instance. Currently, we pursue this direction by developing the above-mentioned hybrid model. This model will have the capability of describing the plasma–beam transition region without the requirement of an interface tracking procedure. This model will be presented and discussed in future work.

Acknowledgments

This work has received the support of the Comissariat à l'Energie Atomique (Center of Bruyères-le-Châtel). The authors thank J. Segré, F. Assous and K.-C. Le Thanh (CEA), D. Payan (CNES) and J.-F. Roussel (ONERA) for their support and encouragements. Support by the European network HYKE, funded by the EC as contract HPRN-CT-2002-00282, is also acknowledged.

Appendix A. Proofs

A.1. Proof of Proposition 3.1

We prove it by induction. Let assume that the quasi-neutrality holds and that the current is a constant at time t^n:

$$\forall k, \quad n_{i_k}^n = n_{e_k}^n = n_k^n, \quad \text{and} \quad (nu_i)_k^n - (nu_e)_k^n = j^n. \tag{A.1}$$

The two-fluid scheme for the computation of ion and electron densities gives, for all k,

$$n_{i_k}^{n+1} = n_{i_k}^n - \frac{\Delta t^n}{\Delta x}\Big((nu_i)_{k+1/2} - (nu_i)_{k-1/2}\Big)^n, \tag{A.2}$$

$$n_{e_k}^{n+1} = n_{e_k}^n - \frac{\Delta t^n}{\Delta x}\Big((nu_e)_{k+1/2} - (nu_e)_{k-1/2}\Big)^n. \tag{A.3}$$

We briefly recall that the HLLE Riemann solver is given by (see e.g. [55] for the details)

$$(nu_{i,e}^n)_{k+1/2} = \frac{1}{\lambda_{+_k} - \lambda_{-_k}}\left(\lambda_{+_k}(nu_{i,e})_k - \lambda_{-_k}(nu_{i,e})_{k+1} + \lambda_{+_k}\lambda_{-_k}(n_{i,e_k} - n_{i,e_{k+1}})\right)^n, \tag{A.4}$$

where λ_{+_k} and λ_{-_k} are defined in [55] (their values do not affect the result). Then, we have for all k,

$$\begin{aligned}
n_{i_k}^{n+1} - n_{e_k}^{n+1} &= \frac{\Delta t^n}{\Delta x}\Big((nu_e)_{k+1/2} - (nu_e)_{k-1/2} - (nu_i)_{k+1/2} + (nu_i)_{k-1/2}\Big)^n, \\
&= \frac{\Delta t^n}{\Delta x(\lambda_{+_k} - \lambda_{-_k})^n}\left[\left(\lambda_{+_k}(nu_e)_k - \lambda_{-_k}(nu_e)_{k+1} + \lambda_{+_k}\lambda_{-_k}(n_k - n_{k+1})\right)\right. \\
&\quad \left. - \left(\lambda_{+_k}(nu_i)_k - \lambda_{-_k}(nu_i)_{k+1} + \lambda_{+_k}\lambda_{-_k}(n_k - n_{k+1})\right)\right]^n \\
&\quad + \frac{\Delta t^n}{\Delta x(\lambda_{+_{k-1}} - \lambda_{-_{k-1}})^n}\left[\left(\lambda_{+_{k-1}}(nu_i)_{k-1} - \lambda_{-_{k-1}}(nu_i)_k + \lambda_{+_{k-1}}\lambda_{-_{k-1}}(n_{k-1} - n_k)\right)\right. \\
&\quad \left. - \left(\lambda_{+_{k-1}}(nu_e)_{k-1} - \lambda_{-_{k-1}}(nu_e)_k + \lambda_{+_{k-1}}\lambda_{-_{k-1}}(n_{k-1} - n_k)\right)\right]^n, \\
&= \frac{\Delta t^n}{\Delta x}\left(\frac{\lambda_{-_k} j_{k+1} - \lambda_{+_k} j_k}{\lambda_{+_k} - \lambda_{-_k}} + \frac{\lambda_{+_{k-1}} j_{k-1} - \lambda_{-_{k-1}} j_k}{\lambda_{+_{k-1}} - \lambda_{-_{k-1}}}\right)^n.
\end{aligned} \tag{A.5}$$

The current is a constant at time t^n, i.e. $\forall k,\ j_k^n = j_{k+1}^n = j_{k-1}^n = j^n$, then (A.5) implies $n_{i_k}^{n+1} - n_{e_k}^{n+1} = 0$. Since the hypothesis (A.1) is verified at initial time, this gives the result. □

A.2. Modal analysis for a uniform plasma perturbation case

A.2.1. Proof of Proposition 4.1

We consider the Euler–Poisson system (2.13)–(2.17) linearized about U^0. It is given by: $\forall x \in \mathbb{R},\ \forall t > 0$

$$(n_i)_t + (u_i)_x = 0, \tag{A.6}$$

$$(n_e)_t + (u_e)_x + u_D(n_e)_x = 0, \tag{A.7}$$

$$(u_i)_t + \gamma_i T_i^0 (n_i)_x = E, \tag{A.8}$$

$$\varepsilon(u_e)_t + \gamma_e T_e^0 (n_e)_x + \varepsilon u_D (u_e)_x = -E, \tag{A.9}$$

$$\lambda\eta E_x = n_i - n_e. \tag{A.10}$$

Let W be equal to (n_i,n_e,u_i,u_e), and consider plane-wave solutions $W = \bar{W}\exp[i(kx - \omega t)]$ of (A.6)–(A.10). Then, we have

$$-\omega\bar{W} + A(k)\bar{W} = 0, \tag{A.11}$$

where

$$A(k) = \begin{pmatrix} 0 & 0 & k & 0 \\ 0 & ku_D & 0 & k \\ k\gamma_i T_i^0 + \frac{1}{k\lambda\eta} & \frac{-1}{k\lambda\eta} & 0 & 0 \\ \frac{-1}{\varepsilon k\lambda\eta} & \frac{k\gamma_e T_e^0}{\varepsilon} + \frac{1}{\varepsilon k\lambda\eta} & 0 & ku_0 \end{pmatrix}. \tag{A.12}$$

This system admits non-zero solutions iff $\det(A(k) - \omega I) = 0$, which leads to the dispersion equation (4.1). □

A.2.2. Proof of proposition 4.2

Equation (4.1) is written as a polynomial equation of the fourth degree for the variable ω with real coefficients. Hence, for a fixed value of k, if this equation admits a complex solution ω, then its complex conjugate is a solution too. If there exists at least one solution of (4.1) with $\mathrm{Im}(\omega) < 0$, then the solution is unstable. To obtain a tractable solution, we suppose that $T_i^0 = 0$. The dispersion equation (4.1) becomes

$$D_\omega(k) = k^2\left[\varepsilon u_D^2 - \gamma_e T_e^0\right]\left[\lambda\eta\omega^2 - 1\right] - 2k\varepsilon\omega u_D\left[\lambda\eta\omega^2 - 1\right] + \omega^2\left[\varepsilon(\lambda\eta\omega^2 - 1) - 1\right] = 0. \tag{A.13}$$

We solve this equation for k as a function of ω. The reduced discriminant of $D_\omega(k)$ is

$$\Delta' = (\lambda\eta)^2\varepsilon\gamma_e T_e^0\omega^2(\omega^2 - 1/(\lambda\eta))(\omega^2 - a),$$

where

$$a = ((1+\varepsilon)\tau_e^0 - \varepsilon u_D^2)/(\lambda\eta\varepsilon\gamma_e T_e^0).$$

Then, the solutions of the dispersion equation (A.13) are

$$k_\pm(\omega) = \frac{1}{\varepsilon u_D^2 - \tau_e^0}\left[\varepsilon u_D\omega \pm |\omega|\left(\varepsilon\gamma_e T_e^0 + \frac{\varepsilon u_D^2 - \gamma_e T_e^0}{\lambda\eta\omega^2 - 1}\right)^{1/2}\right].$$

Considering ω as a parameter, the solution $k_\pm$ is real if $\Delta' > 0$ which is equivalent to either

- (i) $a < 0$ and $|\omega| > 1/\sqrt{\lambda\eta}$,
- (ii_1) $a > 1/\lambda\eta$ and $|\omega| < 1/\sqrt{\lambda\eta}$, ($\mathrm{ii}_2$) $a > 1/\lambda\eta$ and $|\omega| > \sqrt{a}$,
- (iii_1) $0 < a < 1/\lambda\eta$ and $|\omega| < \sqrt{a}$, (iii_2) $0 < a < 1/\lambda\eta$ and $|\omega| > 1/\sqrt{\lambda\eta}$.

Then, we study the behavior of k_+ and k_- when ω reaches the bounds of the definition domain. When ω tends to $\pm 1/\sqrt{\lambda\eta}$, k_+ tends to $+\infty$ and the solution k_- tends to $-\infty$. When ω tends to $\pm\infty$, the solution $k_\pm$ is such that $k_\pm \sim (\varepsilon u_D\omega \pm |\omega|\sqrt{\varepsilon\gamma_e T_e^0})/(\varepsilon u_D^2 - \gamma_e T_e^0)$. We deduce the following limits:

- If $a < 1/\lambda\eta$, when ω tends to ∞, k_+ tends to ∞ and k_- tends to ∞. When ω tends to $-\infty$, k_+ tends to $-\infty$ and k_- tends to $-\infty$.
- If $a > 1/\lambda\eta$, when ω tends to ∞, k_+ tends to $-\infty$ and k_- tends to ∞. When ω tends to $-\infty$, k_+ tends to $-\infty$ and k_- tends to ∞.

Note that if $k = 0$, the dispersion equation (4.1) gives

$$\varepsilon\lambda\eta\omega^4 = (1+\varepsilon)\omega^2.$$

Then, $\omega = 0$ is a root of order 2 and $\omega_\pm = \pm(\frac{1}{\lambda\eta} + \frac{1}{\lambda\eta\varepsilon})^{1/2}$ are single roots. We remark that this result does not depends on T_i^0.

This study permits to have a qualitative representation of the dispersion curve. We represent $k_+(\omega)$ and $k_-(\omega)$ in Figs. 11 and 12. To analyze the stability, the process is the following. If for a given $k_0 \in \mathbb{R}^*$, the curve $k = k_0$ has four intersection points with the curve $k_\pm(\omega)$, then there are four real roots of the dispersion equation (A.13) and the solution is stable. Otherwise, there exists a complex root of (A.13) with a positive imaginary part and the solution is unstable.

- *First case* (see Fig. 11): If $a < 0$ which is equivalent to $u_D^2 > (1+\varepsilon)\gamma_e T_e^0/\varepsilon$, and $k > 0$, the solution is stable if k is sufficiently large. Otherwise, it is unstable. We note that in the limit $\lambda\eta \to 0$, all the roots go to infinity. Then, the solution at the quasi-neutral limit is unconditionally unstable.
- *Second case* (see Fig. 12): If $a > 0$ which is equivalent to $u_D^2 < (1+\varepsilon)\gamma_e T_e^0/\varepsilon$, and $k > 0$, two configurations are possible
  - (a) $a > 1/\lambda\eta$ which is equivalent to $u_D^2 < \gamma_e T_e^0/\varepsilon$: The solution is stable for all k.
  - (b) $a < 1/\lambda\eta$ which is equivalent to $\gamma_e T_e^0/\varepsilon < u_D^2$: There exist k_1 and k_2 such that the solution is unstable for $k \in]k_1,k_2[$ and stable otherwise.

We remark that in both cases, the high frequency modes corresponding to $|\omega| > \max(1/\sqrt{\lambda\eta}, \sqrt{a})$ tend to infinity when $\lambda\eta \to 0$, but low frequency modes remain. Hence, the solution at the quasi-neutral limit is stable. □

A.2.3. Proof of Proposition 4.3

The quasi-neutral formulations are formally equivalent. Therefore, we consider the one-fluid formulation ((2.38)–(2.40)) linearized about U^0. It is given by: $\forall x \in \mathbb{R},\ \forall t > 0$

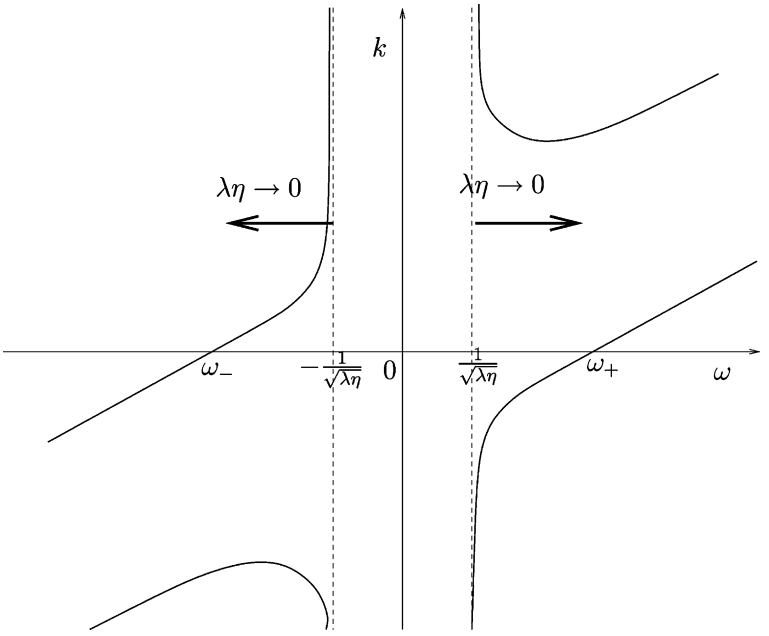

Fig. 11. Dispersion curve $D(\omega,k) = 0$ with $T_i^0 = 0$ in the plane (ω,k) if $u_D^2 > (1+\varepsilon)\gamma_e T_e^0/\varepsilon$. The solution is stable if k is sufficiently large.

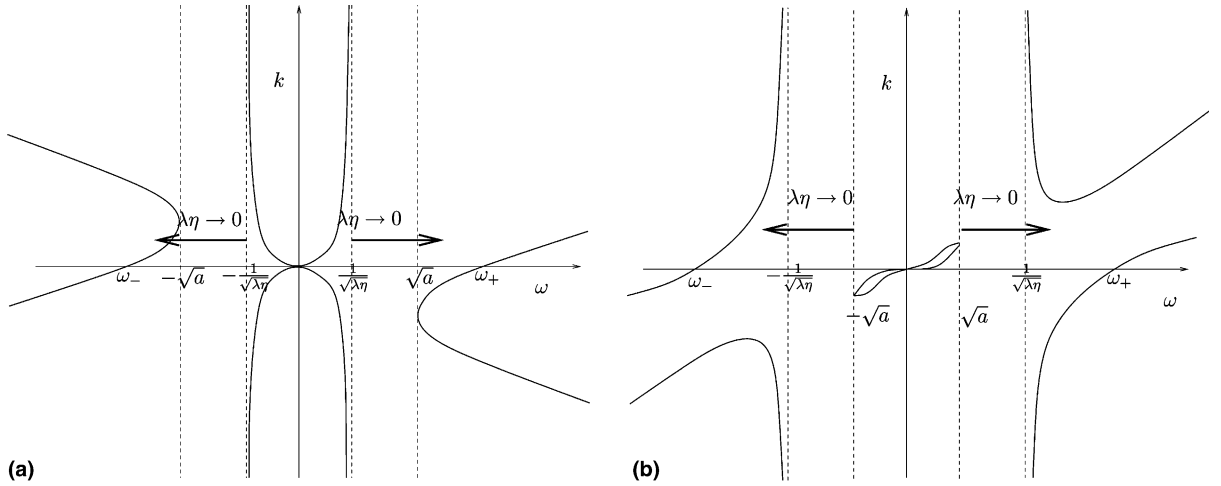

Fig. 12. Dispersion curves $D(\omega,k) = 0$ with $T_i^0 = 0$ in the plane (ω,k) if $u_D^2 < (1+\varepsilon)\gamma_e T_e^0/\varepsilon$. Left: case $u_D^2 < \gamma_e T_e^0/\varepsilon$. Right: case $\gamma_e T_e^0/\varepsilon < u_D^2$.

$$(n_i)_t + (u_i)_x = 0, \tag{A.14}$$

$$(u_i)_t + \frac{1}{(1+\varepsilon)}\left(\gamma_i T_i^0 + \gamma_e T_e^0 - \varepsilon u_D^2\right)(n_i)_x + \frac{2\varepsilon u_D}{1+\varepsilon}(u_i)_x = 0, \tag{A.15}$$

$$j_x = 0. \tag{A.16}$$

Let W be equal to (n_i,u_i), and consider plane-wave solutions $W = \bar{W}\exp[i(kx - \omega t)]$ of (A.14)–(A.16). Then, we have

$$-\omega\bar{W} + B(k)\bar{W} = 0, \tag{A.17}$$

where

$$B(k) = \begin{pmatrix} 0 & k \\ k\frac{\gamma_i T_i^0 + \gamma_e T_e^0}{(1+\varepsilon)} - k\frac{\varepsilon u_D^2}{(1+\varepsilon)} & 2k\varepsilon u_D \end{pmatrix}. \tag{A.18}$$

This system admits non-zero solutions iff $\det(B(k) - \omega I) = 0$, which leads to the dispersion equation (4.2). □

A.2.4. Proof of Proposition 4.4

The starting point of the proof is the dispersion equation (4.2) written as a polynomial equation

$$D_k(\omega) = \omega^2 - 2\omega\frac{k\varepsilon u_D}{1+\varepsilon} - \frac{k^2}{1+\varepsilon}\left(\gamma_i T_i^0 + \gamma_e T_e^0 - \varepsilon u_D^2\right) = 0.$$

We note that $D_k(\omega)$ is a polynomial function of degree 2. Then, ω can be parametrized by k following

$$\omega_\pm = k\frac{\varepsilon u_D}{1+\varepsilon} \pm |k|\frac{\sqrt{\Delta'}}{1+\varepsilon},$$

with

$$\Delta' = \varepsilon^2 u_D^2 + (1+\varepsilon)(\gamma_i T_i^0 + \gamma_e T_e^0 - \varepsilon u_D^2).$$

The solution is stable iff $\Delta' > 0$, i.e.

$$(1+\varepsilon)(\gamma_i T_i^0 + \gamma_e T_e^0) - \varepsilon u_D^2 > 0,$$

which concludes the linear stability analysis. □

References

[1] N. Ben Abdallah, S. Mas-Gallic, P.A. Raviart, Analysis and asymptotics of a one-dimensional ion extraction model, Asymptotic Anal. 10 (1995) 1–28.
[2] Yu.A. Berezin, V.N. Khudick, M.S. Pekker, Conservative finite difference schemes for the Fokker–Planck equation not violating the law of an increasing entropy, J. Comput. Phys. 69 (1987) 163–174.
[3] S.I. Braginskii, Transport processes in a plasma, in: M.A. Leontovitch (Ed.), Reviews of Plasma Physics, vol. 1, 1965.
[4] C. Buet, S. Cordier, P. Degond, M. Lemou, Fast algorithms for numerical, conservative and entropy approximations of the Fokker–Planck–Landau equation, J. Comput. Phys. 133 (1997) 310–322.
[5] F.F. ChenIntroduction to Plasma Physics and Controlled Fusion, vol. 1, Plenum Press, New York, 1974.
[6] M. Cho, D.E. Hastings, Dielectric charging process and arcing rates of high voltage solar arrays, J. Spacecraft Rockets 28 (1990) 698–706.
[7] S. Cordier, E. Grenier, Quasineutral limit of Euler–Poisson system arising from plasma physics, Commun. Partial Differential Equations 25 (5–6) (2000) 1099–1113.
[8] P. Crispel, P. Degond, C. Parzani, M.-H. Vignal, Trois formulations d'un modèle de plasma quasi-neutre avec courant non-nul, C. R. Acad. Sci. Paris 338 (2004) 327–332.
[9] P. Crispel, P. Degond, M.-H.Vignal, Thermal effects in plasma expansion problems, in preparation.
[10] N. Crouseilles, F. Filbet, Numerical approximation of collisional plasmas by high order methods, J. Comput. Phys. 201 (2004) 546–572.
[11] P. Degond, The Child–Langmuir law in the kinetic theory of charged-particles. Part 1, Electron flows in vacuum, in: B. Perthame (Ed.), Advances in Kinetic Theory, World Scientific, Singapore, 1994, pp. 3–44.
[12] P. Degond, S. Jaffard, F. Poupaud, P.A. Raviart, The Child–Langmuir asymptotic of the Vlasov–Poisson equation for cylindrically or spherically symmetric diodes, Math. Methods Appl. Sci 19 (1996) 287–340.
[13] P. Degond, C. Parzani, M.H. Vignal, Un modèle d'expansion de plasma dans le vide, C. R. Acad. Sci. Paris 335 (4) (2002) 399–404.
[14] P. Degond, C. Parzani, M.-H. Vignal, A one-dimensional model of plasma expansion, Math. Comput. Modelling 38 (2003) 1093–1099.
[15] P. Degond, C. Parzani, M.H. Vignal, Plasma expansion in vacuum: modeling the breakdown of quasineutrality, SIAM Multiscale Modeling Simul. 2 (2003) 158–178.
[16] P. Degond, C. Parzani, M.-H. Vignal, On plasma expansion in vacuum, in: P. Colli, C. Verdi, A. Visintin (Eds.), Free Boundary Problems: Theory and Applications, International Series of Numerical Mathematics, vol. 147, Birkhäuser, Basel, 2004, pp. 103–112.
[17] P. Degond, P.F. Peyrard, G. Russo, Ph. Villedieu, Polynomial upwind schemes for hyperbolic systems, C. R. Acad. Sci. Paris 328 (1999) 479–483.
[18] P. Degond, P.A. Raviart, An asymptotic analysis of the one-dimensional Vlasov Poisson system: the Child–Langmuir law, Asymptotic Anal. 4 (1991) 187–214.
[19] P. Degond, R. Talaalout, M.H. Vignal, Electron transport and secondary emission in a surface of a solar cell, comptes-rendus de la confèrence multipactor, RF and DC corona and passive intermodulation in space RF hardware, ESTEC, Noordwijk, The Netherlands, September 4-6, 2000.
[20] E.M. Epperlein, Implicit and conservative difference schemes for the Fokker–Planck equation, J. Comput. Phys. 112 (1994) 291–297.
[21] F. Filbet, L. Pareschi, Numerical method for the accurate solution of the Fokker–Planck–Landau equation in the non homogeneous case, J. Comput. Phys. 179 (2002) 1–26.
[22] R.N. Franklin, J.R. Ockendon, Asymptotic matching of plasma and sheath in an active low pressure discharge, J. Plasma Phys. 4 (1970) 3521–3528.
[23] E. Godlewski, P.A. Raviart, Numerical Approximation of Hyperbolic Systems of Conservation Laws, Springer, Berlin, 1996.
[24] S.Y. Ha, M. Slemrod, Global existence of plasma ion sheaths and their dynamics, Commun. Math. Phys. 238 (2004) 143–186.
[25] D.E. Hastings, M. Cho, H. Kuninaka, Arcing rates for high voltage solar arrays: theory, experiments and predictions, J. Spacecraft Rockets 29 (1992) 538–554.

[26] D.E. Hastings, G. Weyl, D. Kaufman, Threshold voltage for arcing on negatively biased solar arrays, J. Spacecraft Rockets 27 (1990) 539–544.
[27] I. Katz, D.B. Snyder, Mechanism for spacecraft charging initiated destruction of solar arrays in GEO, AIAA 98-1002, 36th Aerospace Sciences Meeting and Exhibit, Reno, NV.
[28] I. Katz, D.B. Snyder, E.A. Robertson, ESD triggered solar array failure mechanism, 6th spacecraft charging technology conference, AFRL-VS-TR-20001578, September 2000.
[29] V.F. Kovalev, V.Yu. Bychenkov, Analytic solutions to the Vlasov equations for expanding plasmas, Phys. Rev. Lett. 90 (2003) 185004.
[30] Ya.E. Krasik, A. Dunaevsky, A. Krokhmal, J. Felsteiner, Emission properties of different cathodes at $E < 10^5$ V/cm, J. Appl. Phys. 89 (2001) 2379–2399.
[31] I. Langmuir, K.T. Compton, Electrical discharges in gases, part II, fundamental phenomena in electrical discharges, Rev. Modern Phys. 3 (1931) 191–257.
[32] P. Lascaux, R. Théodor, Analyse numérique matricielle appliquée à l'art de l'ingénieur, Masson, 1993.
[33] G.A. Mesyats, Explosive Electron Emission, URO Press, Ekaterinburg, 1998.
[34] R.B. Miller, Mechanism of explosive electron emission for dielectric fiber (velvet) cathodes, J. Appl. Phys. 84 (1998) 3880–3889.
[35] K. Nanbu, S. Yonemura, Weighted particles in Coulomb collision simulations based on the theory of a cumulative scattering angle, J. Comput. Phys. 145 (1998) 639–654.
[36] L. Pareschi, G. Russo, G. Toscani, Fast spectral methods for Fokker–Planck–Landau collision operator, J. Comput. Phys. 165 (2000) 216–236.
[37] S.E. Parker, R.J. Procassini, C.K. Birdsall, A suitable boundary condition for bounded plasma simulation without sheath resolution, J. Comput. Phys. 104 (1993) 41–49.
[38] D.E. Parks, G.A. Jongeward, I. Katz, V.A. Davis, Threshold determining mechanisms for discharges in high voltage solar arrays, J. Spacecraft Rockets 24 (1987) 367–371.
[39] D. Payan, A model of inverted voltage gradient discharge inducing a secondary arc between cells on a solar array, in: CNES, European Round Table on modelling of S/C-plasma Interactions, 24–25 February 2000, ESA-ESTEC.
[40] M.S. Pekker, V.N. Khudik, Conservative difference schemes for the Fokker–Planck equation, U.S.S.R. Comput. Math. Math. Phys. 24 (1984) 206–210.
[41] I.F. Potapenko, C.A. de Arzevedo, The completely conservative difference schemes for the nonlinear Landau–Fokker–Planck equation, J. Comput. Appl. Math. 103 (1999) 115–123.
[42] K.U. Riemann, The Bohm criterion and sheath formation, J. Phys. D 24 (1991) 493–518.
[43] K.U. Riemann, Th. Daube, Analytical model of the relaxation of a collisionless ion matrix sheath, J. Appl. Phys. 86 (1999) 1201–1207.
[44] V.A. Rozhansky, L.D. Tsendin, Transport Phenomena in Partially Ionized Plasma, Taylor & Francis, London, 2001.
[45] D. Shiffer, M. Ruebush, D. Zagar, M. LaCour, K. Golby, M. Haworth, R. Umstattd, Cathode and anode plasma in short-pulse explosive field-emission cathodes, J. Appl. Phys. 91 (2002) 5599–5603.
[46] M. Slemrod, Shadowing and the plasma–sheath transition layer, J. Nonlinear Sci. 11 (2001) 193–209.
[47] M. Slemrod, Monotone increasing solutions of the Painleve 1 equation $y'' = y^2 + x$ and their role in the stability of the plasma–sheath transition, Eur. J. Appl. Math. 13 (6) (2002) 663–680.
[48] M. Slemrod, The radio frequency driven plasma sheath: asymptotics and analysis, SIAM J. Appl. Math., submitted.
[49] M. Slemrod, N. Sternberg, Quasi-neutral limit for Euler–Poisson system, J. Nonlinear Sci. 11 (2001) 193–209.
[50] D.B. Snyder, D.C. Ferguson, B.V. Vayner, J.T. Galofaro, New spacecraft-charging solar array failure mechanism, in: 6th Spacecraft Charging Technology Conference, AFRL-VS-TR-20001578, September, 2000.
[51] J.D. Soldi, D.E. Hastings, D. Hardy, D. Guidice, K. Ray, Flight data analysis for the photovoltaic array space power plus diagnostics experiment, J. Spacecraft Rockets 34 (1997) 92–103.
[52] L. Spitzer, R. Härm, Transport phenomena in a completely ionized gas, Phys. Rev. 89 (1953) 977–981.
[53] N. Sternberg, V.A. Godyak, Solving the mathematical model of the electrode sheath in symmetrically driven rf discharges, J. Comput. Phys. 111 (1994) 347–353.
[54] H. Sze, J. Benford, W. Woo, B. Harteneck, Dynamics of a virtual cathode oscillator driven by a pinched diode, Phys. Fluids 29 (1986) 3873–3880.
[55] E.F. Toro, Riemann Solvers and Numerical Methods for Fluid Dynamics, Springer, Berlin, 1999.
[56] J.A. Vaughn, M.R. Carruth, I. Katz, M.J. Mandell, G.A. Jongeward, Electrical breakdown currents on large spacecrafts in low earth orbit, J. Spacecraft Rockets 31 (1994) 31–54.
[57] M. Yatsuzuka, D. Young, Plasma effects on electron beam focusin and microwave emission in a virtual cathode oscillator, IEEE Trans. Plasma Sci. 26 (1998).